Biophysical Reviews and Letters **5** (2010) 163-208

Chemomechanical coupling and stochastic thermodynamics of the F_1-ATPase molecular motor with an applied external torque

E. Gerritsma and P. Gaspard
Center for Nonlinear Phenomena and Complex Systems,
Université Libre de Bruxelles, Code Postal 231, Campus Plaine, B-1050 Brussels, Belgium

The effects of external torque on the F_1-ATPase rotary molecular motor are studied from the viewpoint of recent advances in stochastic thermodynamics. This motor is modeled in terms of discrete-state and continuous-state stochastic processes. The dependence of the discrete-state description on external torque and friction is obtained by fitting its transition rates to a continuous-angle model based on Newtonian mechanics with Langevin fluctuating forces and reproducing experimental data on this motor. In this approach, the continuous-angle model is coarse grained into discrete states separated by both mechanical and chemical transitions. The resulting discrete-state model allows us to identify the regime of tight chemomechanical coupling of the F_1 motor and to infer that its chemical and mechanical efficiencies may reach values close to the thermodynamically allowed maxima near the stalling torque. We also show that, under physiological conditions, the F_1 motor is functioning in a highly nonlinear-response regime, providing a rotation rate a million times faster than it would be possible in the linear-response regime of nonequilibrium thermodynamics. Furthermore, the counting statistics of fluctuations can be obtained in the tight-coupling regime thanks to the discrete-state stochastic process and we demonstrate that the so-called fluctuation theorem provides a useful method to measure the thermodynamic forces driving the motor out of equilibrium.

Keywords: energy transduction; tight coupling; efficiency; fluctuation theorem.

I. INTRODUCTION

In molecular motors, the transduction of chemical energy into mechanical work is determined by the constraints of the molecular architecture onto motion. In this context, an important issue is to understand how these constraints control the tightness of the chemomechanical coupling and its efficiency. For this purpose, we dispose nowadays of recent advances in the stochastic thermodynamics of nonequilibrium nanosystems.[1–16] On the one hand, the problem of energy transduction can be formulated in terms of the chemical and mechanical thermodynamic forces which induce directionality in the motion of molecular motors.[17] On the other hand, the so-called fluctuation theorems[2–16] allow us to evaluate the probability of backward fluctuations balancing the mean forward motion of nanomotors. These recent results shed a new light on these essential features, which are related to the function of molecular motors in biology.

The purpose of the present paper is to use the recent advances of stochastic thermodynamics in order to characterize the chemomechanical coupling and nonequilibrium fluctuations of the F_1-ATPase rotary molecular motor. The F_1-ATPase is a protein assembly composed of three α- and three β-subunits spatially alternated as a hexamer $(\alpha\beta)_3$ and forming a barrel for the rotation of the shaft made of a γ-subunit.[18,19]

In vivo, this rotary motor is the hydrophilic part of F_oF_1-ATPase which is an enzyme producing adenosine triphosphate (ATP) in mitochondria.[20–22] The F_o part of this protein is embedded in the inner membrane of mitochondria and is rotating as a turbine when a proton current flows through it, across the membrane. This turbine drives the rotation of the γ-subunit inside the hydrophilic F_1 part which stands outside the membrane. This rotation performs the energy transduction from the transmembrane pH difference to the chemical free-energy stored in ATP during its synthesis from adenosine diphosphate (ADP) and inorganic phosphate (P_i) inside the catalytic sites lodged in the β-subunits of F_1-ATPase. Since ATP is the fuel of biological cells, F_1-ATPase plays a central role in bioenergetics and is the focus of fundamental investigations.

In vitro, the F_1 part, hence $(\alpha\beta)_3\gamma$ in composition, can be separated from the F_o part and fixed to a coated coverslip, while an actin filament or a colloidal bead is attached to its γ-shaft.[23–27] The whole assembly forms a nanomotor powered by ATP hydrolysis and rotating in the direction opposite to the one of synthesis (see Fig. 1). With such experimental setup, the motion of this nanomotor has been observed to proceed in steps of 120°, revealing the three-fold symmetry of F_1-ATPase.[23] Furthermore, the experiments have shown that each of these steps is subdivided into two substeps.[24] The first substep is generated by ATP binding to an empty catalytic β-subunit of F_1. The secondary substep follows the hydrolysis of ATP and results into the release of the products ADP and P_i, completing the 120° step.[26,27]

Most remarkably, the rotation of F_1-ATPase can also be controlled experimentally by magnetic tweezers or elec-

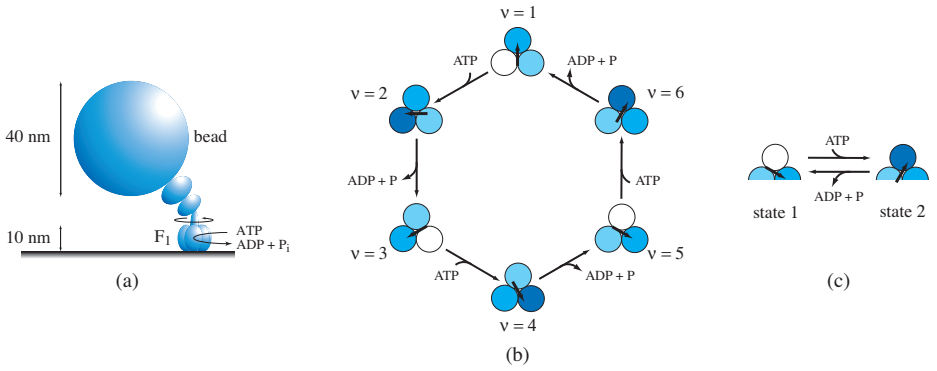

FIG. 1: (a) Schematic representation of the F_1-ATPase nanomotor fixed to a coated coverslip and with a bead of 40-nm diameter attached to its γ-shaft. (b) Diagram of the cycle of the motor. Each $\alpha\beta$-subunit is schematically depicted by a circle and the γ-subunit by an arrow. The γ-subunit rotates by about 90° after ATP binding to an empty catalytic β-subunit (first substep) and by about 30° during the release of ADP and P_i (second substep). (c) Symmetry-reduced diagram with the two states considered in the minimal discrete-state stochastic model.

trorotation inducing an external torque on the γ-shaft.[28–30] In Refs. 28 and 29, a magnetic bead was attached to the γ-subunit and was rotated with external electric magnets, mechanically driving ATP synthesis by F_1-ATPase. In this way, direct evidence was provided that F_1-ATPase may develop high chemomechanical coupling efficiency if the ε-subunit of F_oF_1-ATPase remains attached to the γ-subunit.[29] In Ref. 30, a polystyrene bead dimer was attached to the γ-subunit and was rotated with fast electrorotation. This technique has the advantage to generate constant external torques, which is not the case with magnetic tweezers. These artificial devices play the role of the F_o part which induces *in vivo* the torque responsible for ATP synthesis in mitochondria.

Thanks to these remarkable experiments, the F_1 nanomotor can be externally driven out of equilibrium by two independent thermodynamic forces or affinities: (1) the external torque and (2) the chemical potential difference of ATP hydrolysis which is fixed by the concentrations of ATP, ADP and P_i. These affinities drive two corresponding fluxes which are the mechanical rotation of the γ-subunit and the chemical reaction rate in the catalytic sites of F_1-ATPase. The relationships between the thermodynamic fluxes and forces are fundamental in order to evaluate the degree of chemomechanical coupling that the nanomotor can develop in its different regimes of functioning.[17]

At the nanoscale, the atoms composing the proteins and their environment undergo erratic movements, which persist in spite of the directionality generated out of equilibrium by the thermodynamic forces. Accordingly, stochastic processes are required to describe molecular motors such as the F_1-ATPase. Different levels of description can be adopted depending on the scale of coarse graining.[31]

The finer description is provided by continuous-state stochastic processes where the angle of the γ-subunit is treated as a continuous variable undergoing biased Brownian motion in free-energy potentials corresponding to the different internal states of the motor.[32–39] These stochastic models suppose that the rotation angle obeys a stochastic Newtonian equation of Langevin type and the internal state undergoes random jumps upon each chemical reactive event. Accordingly, the principles of Newtonian mechanics can be used to implement the dependence on the external torque, which is added to the internal torque induced by the current chemical state of the motor and to the Langevin fluctuating torque due to thermal agitation. Such continuous-state stochastic processes are often referred to as ratchet models and they are ruled by coupled Fokker-Planck equations.[31–33] In the present paper, we use the continuous-angle model of Ref. 37, which accurately reproduces the experimental observations of Ref. 24.

Besides, coarser descriptions can also be considered in terms of stochastic jump processes between discrete states.[7,9,11,12,31,40–51] Discrete states can be introduced following different approaches. The basic approach consists in discretizing the continuous variables of Fokker-Planck equations with the aim of setting up a computational method for simulating the process.[43,44] For such purposes, the step size used in the simulation algorithm is meant to be taken as small as possible for convergence towards the continuous process. In other approaches, the discretization is motivated by the observation of distinct steps in the motion of the molecular motor. In this case, the continuous variable of position can be discretized by using the observed step sizes[45–47] or by assuming that the chemical transition rate functions are localized at discrete positions.[41,42] Related aspects concern the separation of different time scales in the dynamics of molecular motors. A first aspect is the general assumption of local thermal equilibrium which implies that the thermal equilibration of the states considered in the stochastic process is fast compared to the transition between the states.[33,52] A second aspect is the relative time duration of chemical and mechanical steps. Indeed, the chemical reactions often take longer than the mechanical steps, which justifies the discretization of the state space in many cases.[48,50] This is in particular the case for the F_1-ATPase motor at low friction where short rotational steps

and substeps are observed between longer dwells controlled by ATP concentration.[24,37] Under such circumstances, a coarse graining could be envisaged, which would relate the continuous-variable description to the discrete-state process, relevant over the time scale of chemical kinetics.[40] Several methods of coarse graining are available: There is the direct numerical method which consists in fitting the rate constants of the discrete model to simulations of the continuous process, as performed in the present paper. There also exist complementary analytical methods, as described in Appendix A. In such coarse-grained descriptions, the reduced stochastic process is no longer a process with both diffusion and jumps, but becomes a pure jump process ruled by a discrete-state master equation.[52,53] Besides the reduction of the description provided by coarse graining, the relationship between both descriptions addresses several issues of principle and is thus important to understand for our purposes.

On the one hand, the assumption that the angle of the γ-subunit is no longer continuous appears as an obstruction to the use of Newtonian mechanics and its principles to determine the dependence on the external torque. Indeed, stochastic jump processes are fully defined in terms of transition rates between the discrete states so that the effects of an external torque or force can only be incorporated by giving appropriate phenomenological dependences to the transition rates.[46,54] In this regard, they are often assumed to have an exponential dependence on the external force or torque,[11,12,31,55–58] although non-exponential dependences are also supposed.[47,48,59–61]

On the other hand, the condition of tight chemomechanical coupling can be expressed in a discrete-state description by assuming that each reactive event is associated with a corresponding rotation of the γ-subunit. We notice that this is not always the case because the discrete-state process can in general include transitions in which a reactive event occurs without mechanical motion or vice versa.[50] The chemomechanical coupling can be tight or loose depending on whether the mechanical motion is directly driven by the reactive events or not.[62] By coarse graining into discrete states which are separated by *both* mechanical steps and ATP hydrolysis transitions, a discrete-model is obtained that has no slip cycle[50] and thus satisfies the tight-coupling condition. Therefore, the comparison of the discrete-state and continuous-angle models of F_1-ATPase allows us to identify the regime of tight coupling and to determine how the external torque may induce a displacement of the effective state of thermodynamic equilibrium.

Furthermore, discrete-state stochastic processes have non-trivial time-dependent fluctuations, which can be studied thanks to their analytic solvability. In this regard, we can use the fluctuation theorem in order to characterize the fluctuations around the directional rotation of the motor. Thanks to an applied external torque, the motor can be driven into regimes where the backward fluctuations are more easily observed than in the absence of external driving. In this way, the counting statistics of random rotations and the symmetry relation of the fluctuation theorem should provide a systematic method to measure not only the mechanical but also the chemical thermodynamic force powering motion in single-molecule experiments.[63]

The paper is organized as follows. In Section II, we present in detail the discrete-state description of the F_1 molecular motor. In Section III, this description is compared with our previous continuous-angle model[37] while coarse graining methods are discussed in Appendix A. In Section IV, we discuss the properties of the F_1 motor in the light of the comparison between the discrete- and continuous-state descriptions and, in particular, the question of the chemomechanical coupling, the thermodynamic efficiencies, and the consequences of the fluctuation theorem. The conclusions are drawn in Section V.

II. DISCRETE-STATE DESCRIPTION

A. Chemistry of the F_1 motor

The F_1 motor is powered by the hydrolysis of ATP into ADP and P_i:

$$\mathrm{ATP} \rightleftharpoons \mathrm{ADP} + \mathrm{P_i} \tag{1}$$

This reaction is driven by the difference of chemical potential $\Delta\mu$ between ATP and the products of hydrolysis:

$$\Delta\mu = \mu_{\mathrm{ATP}} - \mu_{\mathrm{ADP}} - \mu_{\mathrm{P_i}} \tag{2}$$

where the chemical potential μ_{X} is equal to the corresponding Gibbs free energy per molecule defined as

$$\mu_{\mathrm{X}} = \mu^0_{\mathrm{X}} + k_{\mathrm{B}}T \ln \frac{[\mathrm{X}]}{c^0} \tag{3}$$

in terms of the concentration [X] of species X = ATP, ADP, or P_i, the absolute temperature T, Boltzmann's constant $k_{\mathrm{B}} = 1.38 \times 10^{-23}$ J/K, and the reference concentration $c^0 = 1$ mole per liter at which the chemical potential of species X takes its standard value μ^0_{X}.[17]

The standard Gibbs free energy of ATP hydrolysis takes the value $\Delta G^0 = -\Delta\mu^0 = -30.5$ kJ/mol $= -7.3$ kcal/mol $= -50$ pN nm at the temperature of 23°C, the external pressure of 1 atm, and pH 7.[25] We notice that ATP hydrolysis provides a significant amount of free energy of $-\Delta G^0 = 12.2\, k_{\rm B}T$ above the thermal energy $k_{\rm B}T = 4.1$ pN nm. Accordingly, the chemical potential difference (2) can be written as

$$\Delta\mu = \Delta\mu^0 + k_{\rm B}T \ln \frac{[{\rm ATP}]c^0}{[{\rm ADP}][{\rm P_i}]} \simeq k_{\rm B}T \ln \frac{(2\times 10^5\,{\rm M})[{\rm ATP}]}{[{\rm ADP}][{\rm P_i}]} \tag{4}$$

showing that ATP tends to hydrolyze into ADP and P_i. As required, the chemical potential difference vanishes at thermodynamic equilibrium. In the following, the reference concentration c^0 is no longer written, assuming that the concentrations are counted in mole per liter (M).

The kinetic scheme of our model is based on the phenomenological observations of 120° rotation of the γ-shaft per consumed ATP molecule. In accordance with Ref. 24, the first substep of about 90° is induced by the binding of ATP to an empty catalytic site of F_1. The second substep of about 30° is induced by the release of ADP and P_i. The process can be summarized by the following chemical scheme

$$\mathrm{ATP} + \underbrace{[\emptyset, \gamma(\theta)]}_{\text{state 1}} \underset{W_{-1}}{\overset{W_{+1}}{\rightleftharpoons}} \underbrace{[\mathrm{ATP}^\ddagger, \gamma(\theta+90^\circ)]}_{\text{state 2}} \underset{W_{-2}}{\overset{W_{+2}}{\rightleftharpoons}} \underbrace{[\emptyset, \gamma(\theta+120^\circ)]}_{\text{state 1}} + \mathrm{ADP} + \mathrm{P_i} \tag{5}$$

From left to right: In state 1, ATP can bind to an empty ($\emptyset$) β-catalytic site of F_1 with the γ-shaft at angular position θ. State 1 is thus defined by $[\emptyset, \gamma(\theta)]$. Binding of ATP induces the 90° rotation of the γ-shaft, which we represent by $\gamma(\theta + 90^\circ)$ and fills this catalytic site. $ATP^\ddagger$ stands for any transition state of ATP between the initial triphosphate molecule to the products of hydrolysis ADP and P_i before the evacuation of the β-catalytic site. State 2 is thus represented by $[ATP^\ddagger, \gamma(\theta+90^\circ)]$. If F_1 proceeds to hydrolysis, the products ADP and P_i are released, which induces the secondary 30° rotation and empties a β-subunit. This scheme is depicted in Fig. 1c.

In this discrete-state description, the discrete values of the angle of the γ-shaft correspond to the chemical states so that the mechanical motion of the motor is directly controlled by its chemistry. We notice that Eq. (5) does not necessarily represent the same β-subunit during different *real* catalytic states. According to Ref. 24, ADP and P_i are released together, but from a different β-subunit than the ATP binding one. In this case, Eq. (5) represents different β-subunits; one that binds ATP and one that releases ADP and P_i from another ATP molecule previously bound to another β-catalytic subunit. This situation arises in the bi-site and three-site mechanisms of rotation. Furthermore, if the concentration [ATP] is below the nanomolar, F_1 can perform uni-site catalysis.[64] In this other case, Eq. (5) would represent a single β-subunit in its two main catalytic states. The relevance of Eq. (5) to both cases is a consequence of our approach which consists in looking only at the contributions of ATP hydrolysis to the rotation of γ. Very recent experimental observations have shown that ADP and P_i may be released from different β-subunits.[26] If both product molecules are released at different times, a more complete model could be considered by adding a third state to the kinetic scheme. Here, the scheme is simplified by lumping together the two states subsequent to hydrolysis in a regime where the time delay between the releases of ADP and P_i is short enough, as also considered elsewhere.[37]

Since F_1 is a hexamer composed of three β-subunits, the reactions (5) appear three times for the angles $\theta + 120^\circ n$ with $n = 0, 1, 2$, so that the motor has a total of six chemical states. However, by the three-fold symmetry of the F_1 motor, these six states can be regrouped three by three since the process repeats itself similarly every 120° in each β-subunit. We can therefore identify the three states of type 1 together in state 1 and the same for state 2, reducing the motor dynamics to a process with only two discrete states.

According to the mass-action law of chemical kinetics, the transition rates W_ρ in Eq. (5) depend on the molecular concentrations in the solution surrounding the motor as follows

$$W_{+1} = k_{+1}[{\rm ATP}] \tag{6}$$
$$W_{-1} = k_{-1} \tag{7}$$
$$W_{+2} = k_{+2} \tag{8}$$
$$W_{-2} = k_{-2}[{\rm ADP}][{\rm P_i}] \tag{9}$$

where the quantities k_ρ ($\rho = \pm 1, \pm 2$) are the rate constants of the forward and backward reactions of binding and unbinding of ATP or ADP with P_i and, [ATP], [ADP], [P_i] represent the concentrations of each species. k_{+1} is the constant of ATP binding often denoted $k_{\rm on}$ and k_{-1} the ATP unbinding constant $k_{\rm off}$, while k_{+2} is the constant of ATP catalysis denoted $k_{\rm cat}$. The two-state model includes the possibility of ADP and P_i binding and thus ATP synthesis, with the corresponding rate constant k_{-2}. Since the transition rates W_ρ are measured in s^{-1}, the constant k_{+1} has the units of $M^{-1}s^{-1}$, k_{-1} and k_{+2} the units of s^{-1}, and k_{-2} the units of $M^{-2}s^{-1}$.

An important aspect of the experiments with beads or actin filaments attached to the γ-shaft is that the behavior of the molecular motor also depends on the friction coefficient ζ of the attached objects moving in the viscous medium surrounding F_1, as well as on the external torque τ which is applied in some experiments.[28–30] In order to take into account these mechanical aspects in the present discrete-state model, we have to give an appropriate dependence on the friction coefficient ζ and the external torque τ to the rate constants $k_\rho(\zeta,\tau)$ ($\rho=\pm1,\pm2$). In the following, we shall determine these dependences by comparison with the continuous-angle model,[37] in which the mechanical properties are properly described thanks to the principles of Newtonian mechanics. This will be carried out in Section III where the discrete-state model will be completed in this way. We notice that a discrete-state model with six chemical states has been studied in Ref. 9 in the particular case where the external torque is vanishing and for a fixed value of the friction coefficient. Here, our purpose is to investigate situations where the molecular motor is subjected to an external torque to understand how the coupling between chemistry and mechanics can be formulated in terms of the transition rates (6)-(9) of the discrete-state model.

B. Master equation description

The chemistry of F_1 is considered as a stochastic process since the arrivals and departures of each substrate molecule (ATP or ADP with P_i) in the catalytic sites of the motor are random events in time. Accordingly, the time evolution of the molecular motor is described in terms of the probabilities $P_\sigma(t)$ to find it in one or the other of the two states $\sigma=1,2$ of the kinetic scheme (5). These probabilities evolve in time because of the random transitions between both states at each reaction. This time evolution is thus ruled by the master equation:[50,52,53]

$$\frac{dP_\sigma(t)}{dt}=\sum_{\rho,\sigma'}\left[W_\rho(\sigma'|\sigma)P_{\sigma'}(t)-W_{-\rho}(\sigma|\sigma')P_\sigma(t)\right] \tag{10}$$

with a sum over the two reactions $\rho=1,2$ and the two states $\sigma'=1,2$ before the transition $\sigma'\xrightarrow{\rho}\sigma$ or after the reverse transition $\sigma\xrightarrow{-\rho}\sigma'$. The quantity $W_\rho(\sigma'|\sigma)$ is the transition rate per unit time from the state σ' to the state σ due to the reaction ρ, which can be identified with the rate of the corresponding reaction between the two chemical states σ and σ'. The master equation conserves the total probability $\sum_\sigma P_\sigma(t)=1$ for all times t. Using the specific values of the four transition rates of Eq. (5) resumed in Eqs. (6)-(9), we write the time evolution of the states 1 and 2 with respectively empty and occupied catalytic site as

$$\frac{dP_1}{dt} = (W_{-1}+W_{+2})P_2-(W_{+1}+W_{-2})P_1 \tag{11}$$

$$\frac{dP_2}{dt} = (W_{+1}+W_{-2})P_1-(W_{-1}+W_{+2})P_2 \tag{12}$$

with the normalization condition $P_1+P_2=1$ being always satisfied.

The mean consumption rates of the different species are defined by

$$\frac{d}{dt}\langle N_{\rm ATP}\rangle = W_{+1}P_1-W_{-1}P_2 \tag{13}$$

$$\frac{d}{dt}\langle N_{\rm ADP}\rangle=\frac{d}{dt}\langle N_{\rm P_i}\rangle = W_{-2}P_1-W_{+2}P_2 \tag{14}$$

Since the γ-shaft rotates by a substep of 90° during the first reaction $\rho=+1$ and by a substep of 30° during the second reaction $\rho=+2$, the mean angle θ of the γ-shaft evolves in time according to

$$\frac{d}{dt}\langle\theta\rangle=\frac{\pi}{2}\left(W_{+1}P_1-W_{-1}P_2\right)+\frac{\pi}{6}\left(W_{+2}P_2-W_{-2}P_1\right) \tag{15}$$

in radians per second.

Stationary state. The master equation admits a stationary solution such that $(d/dt)P_\sigma^{(\rm st)}=0$. This time-independent solution is obtained for each of the two states as

$$P_1^{(\rm st)} = \frac{k_{-1}+k_{+2}}{k_{+1}[\rm ATP]+k_{-1}+k_{+2}+k_{-2}[\rm ADP][P_i]} \tag{16}$$

$$P_2^{(\rm st)} = \frac{k_{+1}[\rm ATP]+k_{-2}[\rm ADP][P_i]}{k_{+1}[\rm ATP]+k_{-1}+k_{+2}+k_{-2}[\rm ADP][P_i]} \tag{17}$$

where we used the normalization condition $P_1^{(\rm st)} + P_2^{(\rm st)} = 1$. We notice that this state is stationary in the statistical sense because an individual motor continues to fluctuate in time. The probabilities (16)-(17) define the statistical distribution of its fluctuations between the states 1 and 2 after sampling over a long enough lapse of time and over many random realizations.

In the stationary state, the mean rotation rate or angular velocity of the γ-shaft is given by

$$V = \frac{1}{2\pi}\frac{d}{dt}\langle\theta\rangle_{\rm st} = \frac{1}{3}\frac{k_{+1}k_{+2}[\rm ATP] - k_{-1}k_{-2}[\rm ADP][P_i]}{k_{+1}[\rm ATP] + k_{-1} + k_{+2} + k_{-2}[\rm ADP][P_i]} \tag{18}$$

in revolutions per second, and the mean reaction rate by

$$R = \frac{d}{dt}\langle N_{\rm ATP}\rangle_{\rm st} = -\frac{d}{dt}\langle N_{\rm ADP}\rangle_{\rm st} = -\frac{d}{dt}\langle N_{\rm P_i}\rangle_{\rm st} = 3V \tag{19}$$

The relation $R = 3V$ is always satisfied in the discrete-state model. This relation expresses the tight chemomechanical coupling and constitutes a built-in property of this model. In the following, we shall see that this condition is also satisfied for a whole range of control parameter values in the continuous-state model.

Equilibrium state. At thermodynamical equilibrium, all the nonequilibrium constraints vanish. In this case, the stationary solution represents the equilibrium probability $P_\sigma^{(\rm eq)}$ and obeys the detailed balance conditions[65]

$$W_\rho(\sigma'|\sigma)P_{\sigma'}^{(\rm eq)} = W_{-\rho}(\sigma|\sigma')P_\sigma^{(\rm eq)} \tag{20}$$

for all the reactions $\rho = 1, 2$ and all the transitions $\sigma, \sigma' = 1, 2$. As a consequence, the rotation and reaction rates, (18) and (19), vanish under the equilibrium condition:

$$K_{\rm eq} \equiv \frac{k_{-1}k_{-2}}{k_{+1}k_{+2}} = \left.\frac{[\rm ATP]}{[\rm ADP][P_i]}\right|_{\rm eq} \tag{21}$$

defining the equilibrium constant of the hydrolysis reaction.

C. Determination of the rate constants

The motor is in a nonequilibrium stationary state if the equilibrium condition (21) is not satisfied. In this case, the mean velocity (18) does not vanish and can be compared with experimental data[24] or with the continuous-angle model[37] which is complete with respect to the mechanics. In this way, each one of the rate constants k_ρ can be determined by appropriate limits at fixed values of ζ and τ, as explained here below.

First of all, the mean velocity (18) can be rewritten in the following form:

$$V = \frac{V_{\rm max}\,([\rm ATP] - K_{\rm eq}[\rm ADP][P_i])}{[\rm ATP] + K_M + K_P[\rm ADP][P_i]} \tag{22}$$

in terms of the constants

$$V_{\rm max} \equiv \frac{1}{3}\,k_{+2} \tag{23}$$

$$K_M \equiv \frac{k_{-1} + k_{+2}}{k_{+1}} \tag{24}$$

$$K_P \equiv \frac{k_{-2}}{k_{+1}} \tag{25}$$

together with the equilibrium constant $K_{\rm eq}$ defined by Eq. (21). The knowledge of these four constants is equivalent to the one of the four rate constants $k_{\pm1}$ and $k_{\pm2}$. Each one of the three constants (23), (24), and (25) can be determined in a specific regime of functioning of the molecular motor.

The constants (23) and (24) can be determined in the absence of the products of hydrolysis, $[\rm ADP][P_i] = 0$, in which case the velocity follows a typical Michaelis-Menten kinetics:

$$V = \frac{V_{\rm max}[\rm ATP]}{[\rm ATP] + K_M} \tag{26}$$

Here, we see that Eq. (24) is the Michaelis-Menten constant defined as the ATP concentration at which the velocity V equals $V_{\max}/2$.[66] This constant characterizes the crossover between the regime $[\mathrm{ATP}] \ll K_\mathrm{M}$ where the rotation is limited by the slow arrival of ATP molecules and the saturation regime $[\mathrm{ATP}] \gg K_\mathrm{M}$ where the velocity reaches its maximum value fixed by the finite release rate of ADP and $\mathrm{P_i}$. Accordingly, the constant (23) is the maximum angular velocity of the motor, which is reached in a regime where the ATP concentration is large enough with respect to the Michaelis-Menten constant:

$$V_{\max} = \lim_{[\mathrm{ATP}]\to\infty} V \tag{27}$$

the limit meaning that $[\mathrm{ATP}] \gg K_\mathrm{M}$. The Michaelis-Menten constant itself can be determined at low ATP concentrations according to

$$K_\mathrm{M} = \lim_{[\mathrm{ATP}]\to 0} [\mathrm{ATP}] \left(\frac{V_{\max}}{V} - 1 \right) \tag{28}$$

this other limit meaning that $[\mathrm{ATP}] \ll K_\mathrm{M}$.

The third constant (25) characterizes the decrease of the velocity happening if the concentrations of the products ADP and $\mathrm{P_i}$ are increased. As we shall see in the following, it turns out that this constant is larger than the equilibrium constant by several orders of magnitude:

$$K_\mathrm{P} \gg K_\mathrm{eq} \tag{29}$$

Accordingly, the term involving the equilibrium constant in the numerator of Eq. (22) can be neglected. Hence, the constant K_P can be determined in the regime where

$$\frac{[\mathrm{ATP}] + K_\mathrm{M}}{K_\mathrm{P}} \ll [\mathrm{ADP}][\mathrm{P_i}] \ll \frac{[\mathrm{ATP}]}{K_\mathrm{eq}} \tag{30}$$

by taking the difference of the inverses of the velocities at two different concentrations of ADP, keeping fixed the other concentrations:

$$K_\mathrm{P} = V_{\max} \frac{[\mathrm{ATP}]}{[\mathrm{P_i}]} \frac{\Delta(1/V)}{\Delta[\mathrm{ADP}]} \tag{31}$$

with the notation $\Delta X = X_2 - X_1$.

Another consequence of the inequality (29) is obtained by using the definition (21) of the equilibrium constant:

$$k_{-1} = \frac{K_\mathrm{eq}}{K_\mathrm{P}} k_{+2} \ll k_{+2} \tag{32}$$

whereupon the Michaelis-Menten constant (24) is essentially independent of k_{-1} in the present case:

$$K_\mathrm{M} = \frac{k_{+2}}{k_{+1}} \tag{33}$$

and thus directly determines the constant k_{+1} of ATP binding once the constant k_{+2} of product release is obtained thanks to the maximum velocity (23). Subsequently, the constant k_{-2} of ADP and $\mathrm{P_i}$ binding is determined from the constant K_P as explained here above. Finally, the constant k_{-1} of ATP unbinding is determined with the equilibrium constant (21). In summary, we find successively:

$$k_{+2} = 3\, V_{\max} \tag{34}$$

$$k_{+1} = \frac{k_{+2}}{K_\mathrm{M}} \tag{35}$$

$$k_{-2} = k_{+1} K_\mathrm{P} \tag{36}$$

$$k_{-1} = \frac{k_{+1} k_{+2}}{k_{-2}} K_\mathrm{eq} \tag{37}$$

These formulas will be used in Section III to determine the rate constants of the discrete-state model from numerical simulations of the continuous-angle model.[37]

D. Thermodynamics of the F_1 motor

A fundamental requirement is that the description in terms of stochastic processes should be consistent with the laws of thermodynamics. In particular, the nonequilibrium thermodynamics of the motor is essential to understand the chemomechanical coupling.

In stationary states, the entropy production of the motor is given by

$$\frac{d_{\rm i}S}{dt} = \frac{2\pi\tau}{T}\,V + \frac{\Delta\mu}{T}\,R \geq 0 \tag{38}$$

in terms of the so-called thermodynamics forces or affinities, $2\pi\tau/T$ and $\Delta\mu/T$, corresponding to the stationary rotation and reaction rates defined by Eqs. (18) and (19) (see Appendices B and C).[49,50,67–71] All these quantities vanish at thermodynamic equilibrium. Mechanical or chemical energy is supplied from the exterior if the torque τ or the reaction free energy $\Delta\mu$ is non vanishing.

In general, molecular motors can be driven out of equilibrium by either the external torque τ or the molecular concentrations of ATP, ADP and P_i entering $\Delta\mu$, possibly in combination. In this regard, the thermodynamic forces $2\pi\tau/T$ and $\Delta\mu/T$ are two independent control parameters. However, the chemistry and the mechanics of the molecular motor can be tightly coupled as it is the case for the discrete-state model (11)-(12) according to Eq. (19). Under these circumstances, three ATP molecules are consumed per revolution which is expressed by the condition that the ATP consumption rate is three times the velocity, i.e.,

$$\text{tight coupling:} \qquad V = \frac{1}{3}\,R \tag{39}$$

As a consequence, the stationary entropy production (38) becomes

$$\text{tight coupling:} \qquad \frac{1}{k_{\rm B}}\frac{d_{\rm i}S}{dt} = AR \geq 0 \tag{40}$$

with the chemomechanical affinity

$$A \equiv \underbrace{\frac{2\pi}{3}\frac{\tau}{k_{\rm B}T}}_{\text{mechanics}} + \underbrace{\frac{\Delta\mu}{k_{\rm B}T}}_{\text{chemistry}} \tag{41}$$

which is here written in dimensionless form. In the regime of tight coupling, the mechanical and chemical thermodynamic forces are thus no longer independent control parameters but are replaced by the unique chemomechanical affinity (41) (see Appendix D). This affinity vanishes at equilibrium.

By using Eqs. (4) and (21), the equilibrium condition $A = 0$ implies that

$$\begin{aligned} K_{\rm eq} \;&\equiv\; \frac{k_{-1}k_{-2}}{k_{+1}k_{+2}} = \left.\frac{[{\rm ATP}]}{[{\rm ADP}][{\rm P_i}]}\right|_{\rm eq} \\ &=\; \exp\frac{1}{k_{\rm B}T}\left(\Delta G^0 - \frac{2\pi}{3}\tau\right) \simeq 4.9\times10^{-6}{\rm M}^{-1}\exp\left(-\frac{2\pi}{3}\frac{\tau}{k_{\rm B}T}\right) \end{aligned} \tag{42}$$

This result shows that the chemical equilibrium is displaced in the presence of an external torque. *In vivo*, such an external torque comes from the F_o part of ATPase and the transmembrane pH difference in mitochondria. This displacement of equilibrium finds its origin in the chemomechanical coupling achieved in the F_1 rotary motor but happens only if an external torque is enforced on the γ-shaft. Furthermore, we notice that the equilibrium constant has an exponential dependence on the external torque, as deduced from equilibrium thermodynamic considerations.

We also infer that equilibrium thermodynamics gives a constraint allowing us to fix one rate constant if we know the three other constants. However, the three other rate constants should be determined under nonequilibrium conditions (see the previous Subsection II C).

III. COMPARISON WITH THE CONTINUOUS-STATE DESCRIPTION

In this section, we compare the discrete-state description of the previous Section II with the continuous-state model we reported on in Ref. 37. The continuous-state model considers the rotation angle as a continuous random variable

instead of supposing that the angle jumps by a finite amount at each reactive event. Thanks to Newtonian mechanics, the continuous-state description naturally takes into account mechanical aspects, which should otherwise be assumed in a discrete-state model as explained here above. Therefore, the simulation of our continuous-state model[37] can provide the dependence of the rate constants of the discrete-state model on both the friction coefficient ζ and the external torque τ, which is the purpose of the present section.

A. Fokker-Planck equation description

In the continuous-state model,[37] the system is found at a given time t in one of the six chemical states $\nu = 1, 2, ..., 6$ and the γ-shaft at an angle $0 \leq \theta < 2\pi$. There are six chemical states because the three β-subunits can be successively empty or occupied by a molecule of ATP or by the products ADP and P_i of hydrolysis.

Consequently, the system is described by six probability densities $p_\nu(\theta, t)$ normalized according to $\sum_{\nu=1}^{6} \int_0^{2\pi} p_\nu(\theta, t) d\theta = 1$. The time evolution of the probability densities is ruled by a set of six Fokker-Planck equations coupled together by the terms describing the random jumps between the chemical states ν due to the two chemical reactions (ATP binding and release of the products ADP and P_i) and the corresponding reversed reactions[37]

$$\partial_t\, p_\nu(\theta,t) + \partial_\theta\, J_\nu(\theta,t) = \sum_{\rho=1,2} \sum_{\nu'(\neq\nu)} \left[p_{\nu'}(\theta,t)\; w_{\rho,\nu'\to\nu}(\theta) - p_\nu(\theta,t)\; w_{-\rho,\nu\to\nu'}(\theta) \right] \tag{43}$$

where the probability current densities are given by

$$J_\nu(\theta,t) = -D\; \partial_\theta\, p_\nu(\theta,t) + \frac{1}{\zeta} \left[-\partial_\theta U_\nu(\theta) + \tau \right] p_\nu(\theta,t) \tag{44}$$

When the motor is in the chemical state ν, the γ-shaft is subjected to the internal torque $-\partial_\theta U_\nu$ due to the free-energy potential $U_\nu(\theta)$ of the motor with its γ-shaft at the angle θ. Applying an external torque τ to the motor has the effect of tilting the potentials into $U_\nu(\theta) - \tau\theta$ which eases the rotation or makes it harder, depending on the sign of τ.[32,33] Besides the internal and external torques, the γ-shaft is also affected by the Langevin fluctuating torque corresponding to the diffusive term in Eq. (44).

The diffusion coefficient D is expressed in terms of the friction coefficient ζ according to Einstein's relation $D = k_B T/\zeta$. The friction coefficient ζ can be evaluated for a bead attached to the γ-shaft, a bead dimer, or a cylindrical filament, as presented elsewhere.[24,25,37,72] In the case of a bead of radius r attached off-axis with its distance at a distance $x = r \sin\alpha$ from the rotation axis, the friction coefficient is given by

$$\zeta = 2\pi\eta r^3 \left(4 + 3\sin^2\alpha \right) \tag{45}$$

with the water viscosity $\eta = 10^{-9}$ pN s nm^{-2} and $\alpha = \pi/6$.[25,37]

The free-energy potentials $U(\theta)$ and $\tilde{U}(\theta)$ (for respectively the empty and occupied catalytic sites) and $U^\ddagger(\theta)$ and $\tilde{U}^\ddagger(\theta)$ (for respectively the transition states of ATP binding or unbinding and of the release or binding of ADP and P_i) are given by[37]

$$U(\theta) = U_{2n+1}\left(\theta + \frac{2\pi n}{3}\right) = a + b\,\cos\theta + c\,\cos 3\theta \tag{46}$$

$$\tilde{U}(\theta) = U_{2n+2}\left(\theta + \frac{2\pi n}{3}\right) = \tilde{a} + \tilde{b}\,\cos\left(\theta - \frac{\pi}{2}\right) + \tilde{c}\,\cos\left[3\left(\theta - \frac{\pi}{2}\right)\right] \tag{47}$$

$$U^\ddagger(\theta) = U^\ddagger_{2n+1}\left(\theta + \frac{2\pi n}{3}\right) = E^\ddagger + a^\ddagger\,(1 - \cos\theta) \tag{48}$$

$$\tilde{U}^\ddagger(\theta) = U^\ddagger_{2n+2}\left(\theta + \frac{2\pi n}{3}\right) = \tilde{E}^\ddagger + \tilde{a}^\ddagger\left[1 - \cos\left(\theta + \frac{\pi}{6}\right)\right] \tag{49}$$

with $n = 0, 1, 2$ and the parameters of Table I. All these potentials determine the angle-dependent transition rates $w_{\rho,\nu'\to\nu}(\theta)$ given in Table II according to the mass-action law and the Arrhenius law of chemical kinetics.

The parameters of these potentials have been obtained as follows.[37] Using results about the binding of ATP and ADP to β-subunits, several features of the potentials $U(\theta)$ and $\tilde{U}(\theta)$ have already been established in Ref. 24. In particular, the minimum of $\tilde{U}(\theta)$ is above the minimum of $U(\theta)$ by 20 pN nm and the potential $\tilde{U}(\theta)$ decreases by 60 pN nm during the rotation by 90° after ATP binding. Therefore, we have that $\tilde{U}(0) = 80$ pN nm and $\tilde{U}(\pi/2) = 20$ pN nm, if

$U(0) = 0$. Moreover, the shape of both potentials $U(\theta)$ and $\tilde{U}(\theta)$ can be determined from the probability distributions of the angle of the γ-shaft reported in Ref. 24.[37] Although there is no experimental data for the potentials of the transition states, the transitions are expected to happen for specific orientations of the γ-shaft with respect to the hexamer $(\alpha\beta)_3$. The parameters $a^\ddagger$ and $\tilde{a}^\ddagger$ have been fixed on the basis of the fact that transitions may happen at orientations too far from where they are experimentally observed if too small values are given to these parameters.

Once the potentials $U(\theta)$ and $\tilde{U}(\theta)$ and the parameters $a^\ddagger$ and $\tilde{a}^\ddagger$ are fixed, the three combinations $k_0 \exp(-\beta E^\ddagger)$, $\tilde{k}_0 \exp(-\beta \tilde{E}^\ddagger)$, and $G^0_{\rm ADP} + G^0_{\rm P_i}$ remain to be determined from data at a given temperature. The first two of these three crucial numbers are fitted to reproduce the Michaelis-Menten kinetics of the rotation rate versus the ATP concentration (Fig. 3 of Ref. 24), while the third one is used to fit the dependence on the viscous friction (Fig. 2 of Ref. 24). The values of $E^\ddagger$ and $\tilde{E}^\ddagger$ have been obtained by the constraints that the activation energies must be non-negative for all the angles $0 \leq \theta < 2\pi$, in order to satisfy Arrhenius' law. The values of the attempt frequencies k_0 and $\tilde{k}_0$ follow consequently. Finally, we get $G^0_{\rm ATP} = G^0_{\rm ADP} + G^0_{\rm P_i} - \Delta G^0$ in terms of the standard Gibbs free energy of ATP hydrolysis $\Delta G^0 = -50$ pN nm. This explains how the parameters of the continuous-angle model have been determined in Ref. 37 to fit the experimental observations of Ref. 24.

TABLE I: Values of the parameters of the potentials (46)-(49) and transition rates given in Table II for the continuous-angle model (43).

coefficient	value	units
a	272.5	pN nm
b	-291.6	pN nm
c	19.1	pN nm
$\tilde{a}$	80	pN nm
$\tilde{b}$	-52.5	pN nm
$\tilde{c}$	-7.5	pN nm
$E^\ddagger$	125	pN nm
$a^\ddagger$	360	pN nm
$\tilde{E}^\ddagger$	110	pN nm
$\tilde{a}^\ddagger$	900	pN nm
$G^0_{\rm ATP}$	125	pN nm
$G^0_{\rm ADP}$	75	pN nm
$G^0_{\rm P_i}$	0	pN nm
k_0	4.1×10^7	s^{-1}
$\tilde{k}_0$	4.0×10^{12}	s^{-1}

B. Coarse graining into a discrete-state model

The connection with the discrete-state description in terms of the master equation (10) can in principle be established by coarse graining the continuous-angle model into discrete states. These discrete states correspond to the chemical states of the F_1 motor and they can be experimentally identified because the angle θ of the γ-shaft is observed to fluctuate around specific orientations while the motor is dwelling in a given chemical state.[24] In this respect, the probabilities ruled by the master equation (10) can be related to the probability densities of the continuous-state description (43) according to

$$P_\sigma(t) = \sum_{n=0,1,2} \int_0^{2\pi} p_{2n+\sigma}(\theta, t)\, d\theta \tag{50}$$

where the sum takes into account the three-fold symmetry of the F_1 motor, allowing the reduction from the six chemical states $\nu = 2n + \sigma = 1, 2, ..., 6$ of the continuous-angle model to the two states $\sigma = 1, 2$ of the discrete-state model. In this way, a fully discrete description can be inferred from the continuous-state description, as explained in Appendix A. In general, this reduction from one description to the other by the aforementioned coarse graining leads to non-Markovian equations.[73] If there is a net separation of time scales between the dwell times spent in each discrete state and the jump times between two discrete states, the non-Markovian effects become negligible and a description in terms of the Markovian master equation (10) may hold. This is the situation we here consider.

In this case, the transition rates $W_\rho(\sigma'|\sigma)$ of the master equation (10) can in principle be deduced by solving the Fokker-Planck equations (43). We emphasize that the transition rates $W_\rho(\sigma'|\sigma)$ of the master equation (10) do not depend on the continuous angle contrary to the rates $w_{\rho,\nu'\to\nu}(\theta)$ appearing in the Fokker-Planck equations (43). In spite of their conceptual and numerical differences, the transition rates appearing in both descriptions are related to each other as far as the chemical reactions they describe are concerned (see Table II).

TABLE II: Comparison of the transition rates of the discrete model ruled by the master equation (10) with those of the continuous model ruled by the Fokker-Planck equations (43). Each transition rate is associated with a corresponding chemical reaction: ATP binding for $\rho = +1$; ATP unbinding for $\rho = -1$; the release of ADP and P_i for $\rho = +2$; the binding of ADP and P_i for $\rho = -2$. Contrary to the discrete model, the rates of the continuous model depend on the angle θ of the γ-shaft. Moreover, they have an Arrhenius-type dependence on the inverse temperature $\beta = (k_B T)^{-1}$ and the free-energy potentials given by Eqs. (46)-(49).

$W_\rho(\sigma'\|\sigma)$	$w_{\rho,\nu'\to\nu}(\theta)$
$k_{+1}[\mathrm{ATP}]$	$k_0[\mathrm{ATP}]\exp\left\{-\beta\left[U^\ddagger(\theta) - U(\theta) - G^\circ_{\mathrm{ATP}}\right]\right\}$
k_{-1}	$k_0\exp\left\{-\beta\left[U^\ddagger(\theta) - \tilde{U}(\theta)\right]\right\}$
k_{+2}	$\tilde{k}_0\exp\left\{-\beta\left[\tilde{U}^\ddagger(\theta) - \tilde{U}(\theta+\frac{2\pi}{3})\right]\right\}$
$k_{-2}[\mathrm{ADP}][\mathrm{P_i}]$	$\tilde{k}_0[\mathrm{ADP}][\mathrm{P_i}]\exp\left\{-\beta\left[\tilde{U}^\ddagger(\theta) - U(\theta) - G^\circ_{\mathrm{ADP}} - G^\circ_{\mathrm{P_i}}\right]\right\}$

We notice that the rates $w_{\rho,\nu'\to\nu}(\theta)$ of the continuous model (shown in the second column of Table II) only concern the chemical reactions and, therefore, do not depend on the friction coefficient ζ and the external torque τ which only enter in the current densities (44) appearing in the left-hand side of the Fokker-Planck equations (43). In contrast, the rate constants k_ρ of the discrete model (shown in the first column of Table II) necessarily depend on the friction coefficient ζ and the external torque τ, which otherwise would not appear in the master equation (10). Accordingly, we now need to obtain the dependences $k_\rho(\zeta,\tau)$ of the discrete-state rate constants on both friction and external torque, which is our purpose in the next subsection.

C. Dependence of the rate constants on friction and external torque

Here, we determine the dependences of the rate constants k_ρ on both friction and external torque by fitting them to simulations of our continuous-angle model.[37] Since this latter has been fitted to experimental data, the present fitting procedure is comparable to a fitting to the experimental data of Ref. 24. We use the method presented in Subsection II C. With this efficient numerical method, we evaluate successively the rate constants thanks to Eqs. (34)-(37) for different values of the external torque τ and the friction coefficient ζ.

An essential observation is that the rate constants become independent of the friction coefficient ζ at low friction and decrease as the inverse of this coefficient at high friction: $k_\rho \propto \zeta^{-1}$. The motor is functioning in a reaction-limited regime at low friction and in a friction-limited regime at high friction.[37] At high friction, the substeps are no longer visible since rotation is slowed down by friction, in which case the Fokker-Planck equations (43) suggest indeed that the rate constants should scale as ζ^{-1}.

The crossover between the low- and high-friction regimes can be well described by giving the following analytical form to the rate constants:

$$k_\rho(\zeta,\tau) = \frac{1}{\mathrm{e}^{a_\rho(\tau)} + \mathrm{e}^{b_\rho(\tau)}\zeta} \tag{51}$$

The coefficients of the function in the denominator are taken as exponentials of some arbitrary function of τ in order to guarantee the positivity of the rate constants, the friction coefficient ζ being always non-negative. The functions $a_\rho(\tau)$ can be determined in the low-friction regime and the functions $b_\rho(\tau)$ in the high-friction regime. These functions are taken as expansions in powers of τ limited to the second order:

$$a_\rho(\tau) = a_\rho^{(0)} + a_\rho^{(1)}\tau + a_\rho^{(2)}\tau^2 + O(\tau^3) \tag{52}$$

$$b_\rho(\tau) = b_\rho^{(0)} + b_\rho^{(1)}\tau + b_\rho^{(2)}\tau^2 + O(\tau^3) \tag{53}$$

The coefficients of these expansions are fitted in intervals of values of the external torque which are typically $|\tau| < 20$ pN nm. The values of the coefficients of Eqs. (52)-(53) are given in Table III for the rate constants $k_{+1}(\zeta,\tau)$, $k_{+2}(\zeta,\tau)$, and $k_{-2}(\zeta,\tau)$.

TABLE III: Values of the coefficients of the power expansions (52)-(53) of the functions $a_\rho(\tau)$ and $b_\rho(\tau)$ giving the rate constants $k_{+1}(\zeta,\tau)$, $k_{+2}(\zeta,\tau)$, and $k_{-2}(\zeta,\tau)$, according to Eq. (51).

coefficient	$k_{+1}(\zeta,\tau)$	$k_{+2}(\zeta,\tau)$	$k_{-2}(\zeta,\tau)$	units
$a_\rho^{(0)}$	-16.952	-5.973	-19.382	-
$a_\rho^{(1)}$	9.8×10^{-4}	1.7×10^{-4}	1.29×10^{-1}	$(\text{pN nm})^{-1}$
$a_\rho^{(2)}$	5.8×10^{-4}	1.0×10^{-3}	2.8×10^{-4}	$(\text{pN nm})^{-2}$
$b_\rho^{(0)}$	-16.352	-2.960	-18.338	-
$b_\rho^{(1)}$	-6.6×10^{-2}	-2.7×10^{-2}	5.9×10^{-3}	$(\text{pN nm})^{-1}$
$b_\rho^{(2)}$	1.0×10^{-3}	3.6×10^{-4}	-2.1×10^{-4}	$(\text{pN nm})^{-2}$

The last constant for ATP unbinding is finally obtained by using Eq. (37) as

$$k_{-1}(\zeta,\tau)=\frac{k_{+1}(\zeta,\tau)\,k_{+2}(\zeta,\tau)}{k_{-2}(\zeta,\tau)}\exp\frac{1}{k_{\rm B}T}\left(\Delta G^0-\frac{2\pi}{3}\tau\right) \tag{54}$$

with $\Delta G^0=-50$ pN nm.

Table III shows that the rate constants do not always have an exponential dependence on the external torque τ. Although the exponential dependence prevails if the second-order term of the power expansions (52) and (53) is negligible, some cases require corrections in powers of the external torque.

IV. PROPERTIES OF THE F_1 MOTOR

In this section, we report the results obtained from the connections established between the discrete and continuous models of the F_1 motor. On the one hand, the continuous-angle model reproduces the experimental observations of Ref. 24 so that its simulation can serve to test the assumptions of the discrete-state model, in particular, the assumption of tight coupling. On the other hand, the discrete-state model can be treated analytically thanks to its simplicity. In this way, the fitting of the discrete-state model to the continuous one allows us to investigate more closely the properties of the F_1 motor in the regime of validity of the discrete-state model and, especially, the properties of chemomechanical coupling. Furthermore, we present the consequences of the fluctuation theorem when an external torque is applied to the F_1 motor.

A. Tight versus loose chemomechanical coupling

In order to determine the regime of tight coupling between the chemistry and the mechanics of the F_1 motor, both the angular velocity V and the ATP consumption rate R have been simulated with the continuous-angle model (43) for different values of the external torque τ and chemical potential difference $\Delta\mu$. In Fig. 2, we depict the plane $(\tau,\Delta\mu)$ with the curves corresponding to the vanishing of the velocity, $V=0$, and the ATP consumption rate, $R=0$. The value of the external torque where the velocity vanishes is the so-called stalling torque. Since the variations of the chemical potential difference $\Delta\mu$ can only be unidimensional in such a representation, we take a combined variation of the concentrations of the different species as explained in the caption of Fig. 2. The two curves $V=0$ and $R=0$ intersect at the origin $(\tau=0,\Delta\mu=0)$ which is the thermodynamic equilibrium point. We notice that the curve $V=0$ is above the curve $R=0$ in the plane of the chemical potential difference $\Delta\mu$ versus the torque as it should according to the second law of thermodynamics (38).

In the tight-coupling regime, the condition (39) should hold, which implies that the mechanical and chemical affinities τ and $\Delta\mu$ are no longer independent but should combine into the unique chemomechanical affinity (41). In this regime, the vanishing of the rates, $V=0$ and $R=0$, should thus occur on the curve where the chemomechanical affinity (41) vanishes, i.e., along the straight line

$$\Delta\mu=-\frac{2\pi}{3}\tau \tag{55}$$

This is observed in Fig. 2 for values of the external torque extending from zero down to about $\tau\simeq-30$ pN nm and for chemical potential difference from zero up to $\Delta\mu\simeq 14\,k_{\rm B}T$, which delimits the zone where the tight-coupling

assumption is satisfied. Outside this zone for higher values of $\Delta\mu$ or lower values of τ, the F_1 motor is no longer functioning in the tight-coupling regime and the chemomechanical coupling becomes loose.[62]

Since the coincidence of the curves $V = 0$ and $R = 0$ along the straight line (55) is a feature of the discrete-state model (11)-(12), we may expect the F_1 motor to be well described by this model in the aforementioned zone of tight coupling.

B. Rotation rate versus ATP concentration

Random trajectories of the discrete model can be simulated thanks to Gillespie's numerical algorithm.[74,75] Examples of random trajectories are depicted in Fig. 3 for different values of ATP concentration, illustrating the Michaelis-Menten kinetics described by Eq. (26). At low concentrations $[\mathrm{ATP}] \ll K_\mathrm{M} \simeq 17\,\mu\mathrm{M}$, the motor is essentially waiting for the arrival of new ATP molecules with its γ-shaft at some angle $120°n$ (n integer). Instead, at high concentrations $[\mathrm{ATP}] \gg K_\mathrm{M}$, the rotation is limited by the release of the hydrolysis products ADP and P_i from its catalytic sites with its γ-shaft at some angle $90° + 120°n$ (n integer), as clearly seen in Fig. 3. In this respect, the random trajectories of the discrete model reproduce the jumps by 90° and 30° corresponding to the substeps experimentally observed in Ref. 24. We notice, however, that the discrete model cannot reproduce the small-amplitude fluctuations around the dwell angles as the continuous-angle model does.[37]

The crossover between the regime at low ATP concentration and the saturation regime of the Michaelis-Menten kinetics is seen in Fig. 4 where we directly compare Eq. (26) of the discrete model with experimental data from Ref. 24. At low ATP concentrations, the rotation rate is proportional to the ATP concentration while the rotation rate reaches its maximum value of about 130 rev/s in the saturation regime.

In order to appreciate the nonequilibrium thermodynamics of the molecular motor, it is interesting to depict the rotation rate as a function of the affinity (41) instead of the ATP concentration. Indeed, the former is a substitute of the latter since we can express the concentrations in terms of the chemical potentials by Eq. (3) and use the definitions of the chemomechanical affinity (41) and of the equilibrium constant (21) to get

$$[\mathrm{ATP}] = K_\mathrm{eq}[\mathrm{ADP}][\mathrm{P_i}]\,\mathrm{e}^{A} \tag{56}$$

In this way, we recover the equilibrium relation (21) between the concentrations with Eq. (21) in the thermodynamic

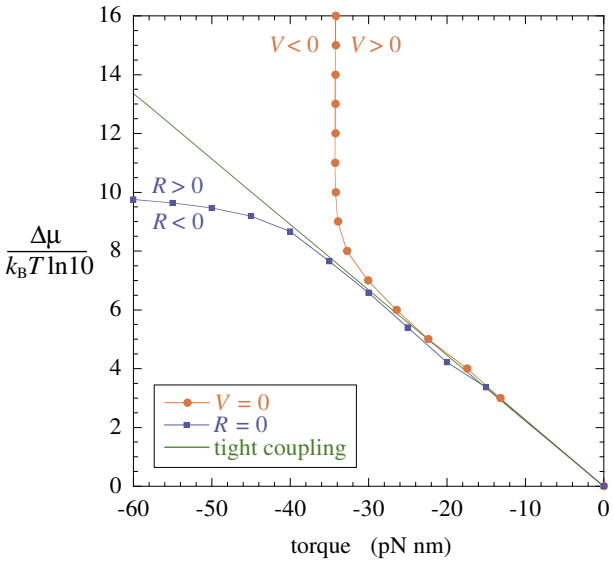

FIG. 2: Chemical potential difference $\Delta\mu$ in units of $k_\mathrm{B}T\ln 10$ versus the external torque τ for the situations where the rotation rate V (circles) and the ATP consumption rate R (squares) vanish in the continuous model (43) and compared with the straight line $\Delta\mu = -2\pi\tau/3$ where the chemomechanical affinity (41) vanishes, $A = 0$. The concentrations are fixed according to $[\mathrm{ATP}] = 4.9 \times 10^{0.8a-11}$ M and $[\mathrm{ADP}][\mathrm{P_i}] = 10^{-0.2a-5}$ M, in terms of the quantity $a = \Delta\mu/(k_\mathrm{B}T\ln 10)$. The bead attached to the γ-shaft has the diameter $d = 2r = 80$ nm and the temperature is of 23 degrees Celsius. The torque where $V = 0$ is called the stall torque. The determination of the curves $V = 0$ and $R = 0$ is difficult close to the thermodynamic equilibrium point ($\tau = 0, \Delta\mu = 0$) because both the rotation rate V and the ATP consumption rate R are very small in this region, which explains the absence of dots close to the origin.

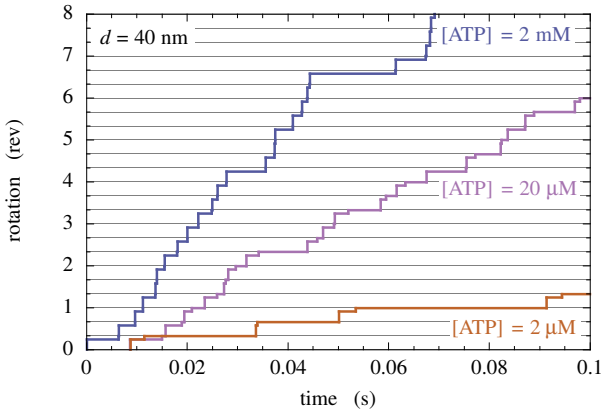

FIG. 3: Simulation of random trajectories of the discrete-state model for [ADP][P_i]=0, a temperature of 23 degrees Celsius, a bead of diameter $d = 2r = 40$ nm, and a zero external torque.

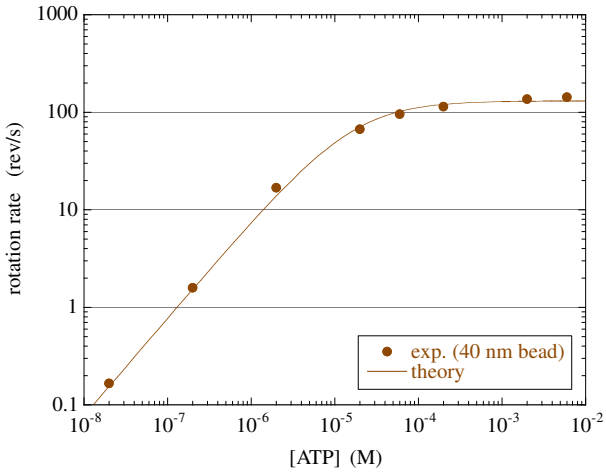

FIG. 4: Mean rotation rate of the γ-shaft of F_1 in revolutions per second, versus the ATP concentration [ATP] in mole per liter for [ADP][P_i]=0. In accordance with the experimental setup,[24] the diameter of the bead is $d = 2r = 40$ nm, the temperature is of 23 degrees Celsius, and the external torque is zero. The circles are the experimental data of Ref. 24. The solid line is the result of numerical simulation of the two-state model.

equilibrium state $A = 0$ corresponding to given concentrations of ADP and P_i. Substituting Eq. (56) into Eq. (22), we obtain the following expression for the rotation rate:

$$V = \frac{V_{\max}\,\left(\mathrm{e}^{A}-1\right)}{\mathrm{e}^{A}-1+\frac{3V_{\max}}{L}} \tag{57}$$

with the constant

$$L \equiv \frac{3V_{\max}K_{\mathrm{eq}}[\mathrm{ADP}][\mathrm{P_i}]}{(K_{\mathrm{eq}}+K_{\mathrm{P}})[\mathrm{ADP}][\mathrm{P_i}]+K_{\mathrm{M}}} \tag{58}$$

This coefficient controls the linear response of the molecular motor because

$$V \simeq \begin{cases} \frac{1}{3}LA & \text{for} \quad A \ll 1 \\ V_{\max} & \text{for} \quad A \gg 1 \end{cases} \tag{59}$$

The analytic form (57) shows that the rotation rate depends on the thermodynamic force A in a highly nonlinear way, in contrast to what is often supposed. The nonlinear dependence is very important as observed in Fig. 5. The linear regime extends around the thermodynamic equilibrium point at $\Delta\mu = 0$ where the function $V(A)$ is essentially flat

because the linear-response coefficient takes the very small value $L \simeq 10^{-5}\,\mathrm{s}^{-1}$ if $[\mathrm{ADP}]\,[\mathrm{P_i}] \simeq 10^{-7}\ \mathrm{M}^2$. Under the physiological conditions $[\mathrm{ATP}] \simeq 10^{-3}$ M, $[\mathrm{ADP}] \simeq 10^{-4}$ M, and $[\mathrm{P_i}] \simeq 10^{-3}$ M,[25] the affinity is about $A \simeq 21.4$ and the rotation rate would take the extremely low value $V \simeq LA/3 \simeq 6.5$ rev/day if the motor was functioning in the linear regime. Remarkably, the nonlinear dependence of Eq. (57) on the affinity A allows the rotation rate to reach the maximum value $V_{\max} \simeq 130$ rev/s under physiological conditions.

C. Rotation in the presence of ATP hydrolysis products

In the presence of ADP and P_i, Eq. (22) shows that the rotation rate decreases, as expected since these products tend to counteract ATP hydrolysis, which powers the motor. This phenomenon is known as ADP inhibition.[24,25] There are two possible causes of the decrease of rotation rate if the concentrations of ADP and $\mathrm{P_i}$ are positive: (1) the term in the numerator of Eq. (22) where the equilibrium constant K_{eq} multiplies $[\mathrm{ADP}][\mathrm{P_i}]$; (2) the term in the denominator of (22) where the constant K_{P} multiplies $[\mathrm{ADP}][\mathrm{P_i}]$. As explained in Subsection II C and can be checked with Table III, the inequality (29) holds by several orders of magnitude so that the main cause of the decrease of the rotation rate is the term in the denominator of Eq. (22) due to the reaction $\rho = -2$ of binding of ADP and $\mathrm{P_i}$ to the catalytic sites of the $\mathrm{F_1}$ motor.

As observed in Fig. 6 which compares the continuous and discrete models, this effect manifests itself above millimolar concentrations of ADP if inorganic phosphate is in millimolar concentration. We notice that the decrease of the rotation rate goes as the inverse of the concentrations of ADP and $\mathrm{P_i}$, $V \propto ([\mathrm{ADP}][\mathrm{P_i}])^{-1}$ as described by Eq. (22) given the fact that the inequality (29) holds.

D. Dependence on friction

Experimentally, friction is controlled by the size of the object which is attached to the shaft of the nanomotor, as depicted in Fig. 1.[23–25] In Fig. 7, we show the effect of friction on the velocity of the motor in the absence of ADP or $\mathrm{P_i}$. At low friction, the velocity saturates exhibiting the reaction-limited regime. At high friction, we observe the rapid decrease of the velocity, which is the feature of the friction-limited regime.[37] In this latter regime, the velocity decreases as the inverse of the friction coefficient $V \propto \zeta^{-1}$ in consistency with the analytical form (51) given to the rate constants. A similar behavior is observed at $[\mathrm{ATP}] = 2$ mM in the saturation regime of the Michaelis-Menten

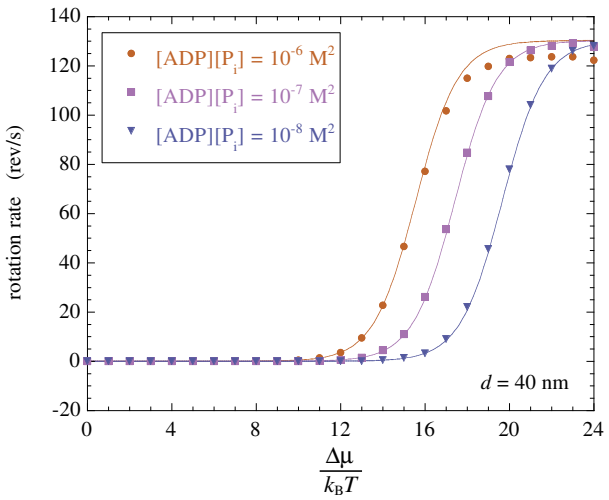

FIG. 5: Mean rotation rate versus the chemical potential difference $\Delta\mu$ in units of the thermal energy $k_{\mathrm{B}}T$. The thermodynamic equilibrium corresponds to $\Delta\mu = 0$. The ATP concentration is given in terms of the chemical potential difference by $[\mathrm{ATP}] = [\mathrm{ADP}][\mathrm{P_i}]\exp[(\Delta\mu - \Delta\mu^0)/(k_{\mathrm{B}}T)] \simeq 4.9 \times 10^{-6}\,\mathrm{M}^{-1}[\mathrm{ADP}][\mathrm{P_i}]\exp[\Delta\mu/(k_{\mathrm{B}}T)]$ since $\Delta\mu^0 = -\Delta G^0 = 50$ pN nm. The results of the discrete model (solid lines) are compared with the continuous model (dots) for three different values of $[\mathrm{ADP}][\mathrm{P_i}]$. The diameter of the bead is $d = 2r = 40$ nm, the temperature 23 degrees Celsius, and the external torque zero. In these conditions, the constants entering the velocity (22) are given by $V_{\max} = 130$ rev/s, $K_{\mathrm{eq}} = 4.9 \times 10^{-6}\,\mathrm{M}^{-1}$, $K_{\mathrm{M}} = 17\,\mu$M, and $K_{\mathrm{P}} = 11.3\,\mathrm{M}^{-1}$.

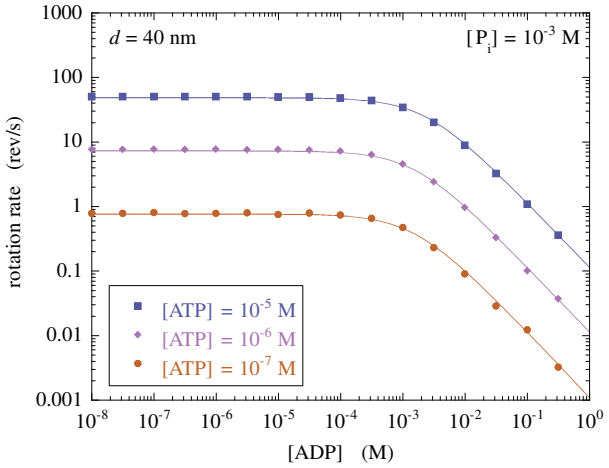

FIG. 6: Mean rotation rate of a bead of diameter $d = 2r = 40$ nm attached to the γ-shaft in revolutions per second versus [ADP] (in mole per liter) and varying ATP concentrations. The concentration of P_i is 10^{-3} M and the temperature of 23 degrees Celsius, and the external torque vanishing. The simulations of the continuous-angle model (squares, diamonds, and circles) are compared with the analytical expression (22) for the discrete model of Table III (lines).

kinetics and at ATP concentrations lower than the Michaelis-Menten constant for [ATP] $= 2\ \mu$M $< K_M = 17\,\mu$M. The agreement is as good as for the continuous-angle model.[37]

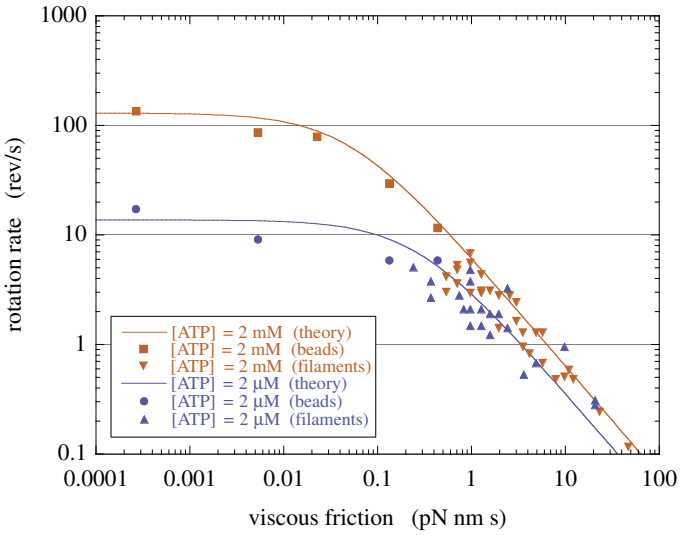

FIG. 7: The mean rotation rate in revolutions per second versus the viscous friction coefficient ζ for a bead, a bead dimer, or a filament attached to the γ-shaft. The circles and triangles are the experimental data in Fig. 2 of Ref. 24 at [ATP] = 2 mM (squares and downward triangles) and [ATP] = 2 μM (circles and upward triangles). The squares and circles correspond to the beads and bead dimers, the triangles to the actin filaments. The solid lines are the results of the present model with [ADP][P_i] = 0, the temperature of 23 degrees Celsius, and zero external torque.

E. Dependence on the external torque

Figure 8 depicts the dependence of the rotation and ATP consumption rates on the external torque τ for both the continuous-angle and discrete-state models, showing their agreement in the interval $|\tau| \lesssim 30$ pN nm. In this interval, the tight-coupling relation $V = R/3$ holds between the mean rotation and reaction rates. This result confirms that the interval $|\tau| \lesssim 30$ pN nm is the range of validity of the discrete model, as already discussed about Fig. 2.

In the interval $|\tau| \lesssim 30$ pN nm, the rates are observed to decrease from a maximum about $\tau \simeq 5$ pN nm. The

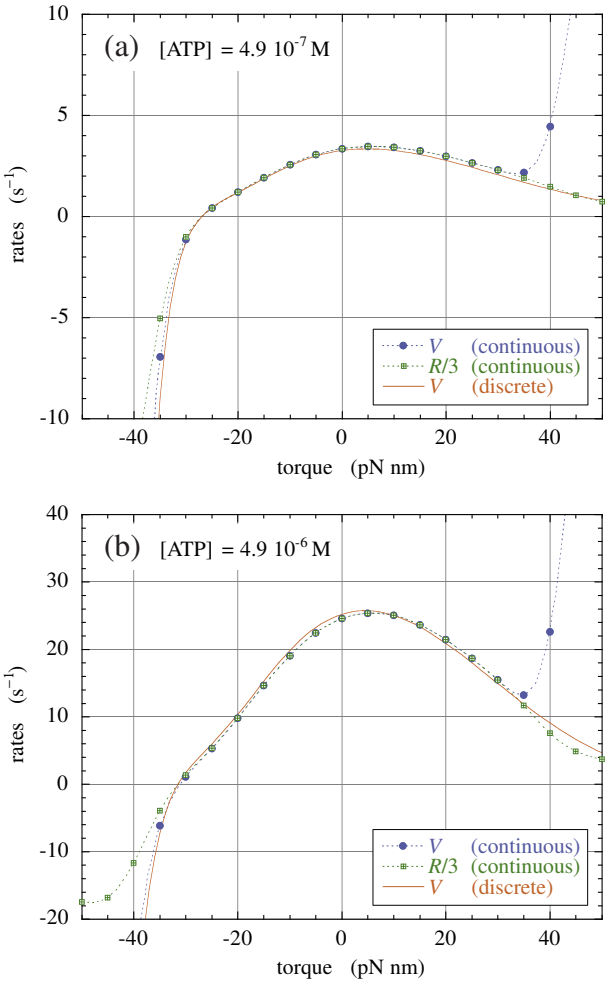

FIG. 8: Mean rotation rate V of the γ-shaft of F_1 in revolutions per second versus the external torque for (a) [ATP] $= 4.9 \times 10^{-7}$ M and (b) [ATP] $= 4.9 \times 10^{-6}$ M (circles for the continuous-state model and solid line for the discrete-state model). The other concentrations are fixed to [ADP] $= 10^{-4}$ M and [P_i] $= 10^{-3}$ M. The squares show the reaction rate R divided by three in order to display the regime of tight coupling where $V = R/3$. The diameter of the bead is $d = 2r = 160$ nm and the temperature of 23 degrees Celsius.

reason is that the external torque is shifting the angle where the γ-shaft is dwelling before the next chemical transition, with respect to the angle where the transition rate is the largest, because the potentials are tilted into $U_\nu(\theta) - \tau\theta$ in Eq. (44). Consequently, the mean rotation and reaction rates decrease as $|\tau|$ increases. Furthermore, for vanishing or moderate values of the external torque $|\tau| \lesssim 30$ pN nm, the potential surfaces have barriers which stop free mechanical motion without chemical transition, tightly coupling in this way mechanical motion to chemical reaction.

For larger values of the external torque $|\tau| \gtrsim 30$ pN nm, the mechanical motion becomes decoupled from the chemical reactions because the potential surfaces $U_\nu(\theta) - \tau\theta$ of the motor are so tilted that the aforementioned barriers disappear.[37] This decoupling between mechanics and chemistry may happen at both negative and positive thresholds for the external torque, as seen in Fig. 8 for the continuous-angle model. Therefore, the tight-coupling condition $V = R/3$ is only observed in the interval $|\tau| \lesssim 30$ pN nm for the continuous-angle model, although it always holds by assumption for the discrete-state model.

Figure 8 also shows the remarkable feature that the discrete model reproduces the phenomenon of stalling torque, according to which rotational motion is stopped at a negative critical value of the external torque opposing the chemical driving. Indeed, Eq. (57) shows that both the rotation and ATP consumption rates vanish at the stalling torque together with the chemomechanical affinity (41). Consequently, we recover the condition (55) giving the stalling torque as

$$\tau_{\rm stall} = -\frac{3}{2\pi}\Delta\mu = -\frac{3}{2\pi}\left(\Delta\mu^0 + k_{\rm B}T\ln\frac{[\rm ATP]}{[\rm ADP][P_i]}\right) \tag{60}$$

in the tight-coupling regime. For $[\mathrm{ADP}][\mathrm{P_i}] = 10^{-7}\,\mathrm{M}^2$, the chemical potential difference takes the values $\Delta\mu = 56.5$ pN nm and $\Delta\mu = 65.9$ pN nm, for respectively $[\mathrm{ATP}] = 4.9 \times 10^{-7}$ M and $[\mathrm{ATP}] = 4.9 \times 10^{-6}$ M. Hence, Eq. (60) gives respectively the stalling torques $\tau_{\rm stall} = -27.0$ pN nm and $\tau_{\rm stall} = -31.5$ pN nm, as indeed observed in Figs. 8a and 8b.

F. Chemical and mechanical efficiencies

Under a negative external torque $\tau < 0$, the $\mathrm{F_1}$ motor can synthesize ATP, in which case the ATP consumption rate as well as the rotation rate are negative, $R < 0$ and $V < 0$. In this regime of ATP synthesis, the chemical efficiency is defined as the ratio of the free energy stored in the synthesized ATP over the mechanical power due to the external torque:

$$\eta_{\rm c} \equiv -\frac{\Delta\mu\, R}{2\pi\tau\, V} \tag{61}$$

such that $0 \leq \eta_{\rm c} \leq 1$.[33]

A mechanical efficiency can similarly be defined in the regime where the rotation is powered by ATP as the inverse of the chemical efficiency[33]

$$\eta_{\rm m} \equiv -\frac{2\pi\tau\, V}{\Delta\mu\, R} \tag{62}$$

The mechanical efficiency satisfies $0 \leq \eta_{\rm m} \leq 1$ in the regime where the external torque is still non-positive while both the rotation and ATP consumption rates are positive, $V > 0$ and $R > 0$.

It is known[33] that the chemical and mechanical efficiencies reach their maximum values under different conditions as shown in Appendix E. However, these conditions coincide in the tight-coupling regime where $R = 3V$ and the efficiencies (61) and (62) become

$$\text{tight coupling:} \qquad \eta_{\rm c} = \frac{1}{\eta_{\rm m}} = -\frac{3\Delta\mu}{2\pi\tau} \tag{63}$$

in agreement with Eq. (E10) derived in Appendix E from the assumption of linear response. In the tight-coupling regime, the chemical and mechanical efficiencies can thus reach the maximal unit value at the stalling torque given by Eq. (60). This remarkable result is observed in Fig. 9 depicting the chemical and mechanical efficiencies versus the external torque under conditions corresponding to the chemical potential difference $\Delta\mu = 56.5$ pN nm.

In the interval $\tau_{\rm stall} = -27.0$ pN nm $< \tau < 0$, the external torque is opposed to the mean rotation rate but the motor consumes ATP, so that the mechanical efficiency (62) is positive. In this interval, the coupling is tight so that the mechanical efficiency computed with the continuous-angle model (squares) agrees with the prediction (63) of tight coupling which holds for the discrete model. Indeed, the mechanical efficiency reaches the unit value at the stalling torque marked by the vertical line.

On the other hand, the motor synthesizes ATP under the action of the external torque for $\tau < \tau_{\rm stall} = -27.0$ pN nm, where the velocity becomes negative and the chemical efficiency (61) positive. As explained above, the motor is no longer in a regime of tight coupling below the stalling torque so that the chemical efficiency computed with the continuous-angle model differs from the prediction (63) of tight coupling. As seen in Fig. 9, the actual chemical efficiency is lower than possible by tight coupling because of the loose chemomechanical coupling below the stalling torque. It is only at the stalling torque that the chemical efficiency (61) tends to the tight-coupling prediction (63) where they reach the unit value.

G. Fluctuations

Since the motor is ruled by a stochastic process, its rotation is random so that backward as well as forward substeps may occur. At equilibrium, backward and forward substeps should be equiprobable by the principle of detailed balance. However, a directionality emerges out of equilibrium because of the energy provided through the thermodynamic forces. This directionality manifests itself in the non-vanishing mean values of the rotation and reaction rates, defining the average forward motion. We notice that the direction of this forward motion still depends on the signs and values of the thermodynamic forces. In such nonequilibrium conditions, the forward substeps are more probable than the backward ones and we may wonder what is the probability that the rotation would proceed

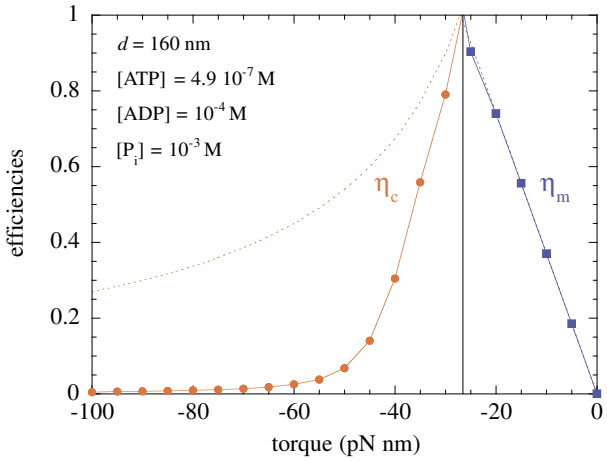

FIG. 9: Chemical efficiency (61) and mechanical efficiency (62) versus the external torque τ in the continuous-state model (respectively circles and squares joined by a solid line) and compared with the prediction (63) of tight coupling (dashed lines). The vertical solid line indicates the stalling torque at $\tau = -27.0$ pN nm. The concentrations are [ATP] $= 4.9 \times 10^{-7}$ M, [ADP] $= 10^{-4}$ M, and [P_i] $= 10^{-3}$ M. The diameter of the bead is $d = 2r = 160$ nm and the temperature of 23 degrees Celsius. These conditions are identical as in Fig. 8a. The predictions of tight coupling (dashed lines) are respectively $\eta_c = \tau_{\rm stall}/\tau$ for $\tau < \tau_{\rm stall}$, and $\eta_m = \tau/\tau_{\rm stall}$ for $\tau_{\rm stall} < \tau < 0$, with $\tau_{\rm stall} = -27.0$ pN nm.

by a certain number S_t of substeps over a given time interval t. Since the substeps are controlled by the reactive events in the tight-coupling regime, we should expect that the number of substeps is related to the number N_t of reactive events occurring during the same time interval.

The counting statistics of these random variables can be carried out by introducing the generating functions of their cumulants. In particular, the generating function of the number N_t of reactive events of ATP hydrolysis over the time interval $[0, t]$ can be defined as

$$Q(\lambda) \equiv \lim_{t\to\infty} -\frac{1}{t} \ln\langle e^{-\lambda N_t}\rangle \tag{64}$$

Following the theory developed in Ref. 9, this generating function is obtained as

$$\begin{aligned} Q(\lambda) \;=\; & \frac{1}{2}\left(W_{+1}+W_{-1}+W_{+2}+W_{-2}\right) - \Big[\frac{1}{4}\left(W_{+1}+W_{-1}+W_{+2}+W_{-2}\right)^2 \\ & + W_{+1}W_{+2}\left(e^{-\lambda}-1\right) + W_{-1}W_{-2}\left(e^{\lambda}-1\right)\Big]^{\frac{1}{2}} \end{aligned} \tag{65}$$

for the stochastic process ruled by the master equations (11)-(12).

All the cumulants of the counting statistics can be obtained by successive derivatives with respect to the parameter λ. In particular, the mean reaction rate (19) is given by

$$R = 3V = \frac{\partial Q}{\partial \lambda}\Big|_{\lambda=0} \tag{66}$$

and the corresponding diffusion coefficient, called dispersion in Ref. 31, by

$$D = -\frac{1}{2}\frac{\partial^2 Q}{\partial \lambda^2}\Big|_{\lambda=0} \tag{67}$$

Besides, the higher cumulants can also be obtained from the generating function (65).

The counting statistics has a remarkable symmetry finding its origin in the underlying microreversibility and expressed by the fluctuation theorems, which have been proved for different types of random variables in transient or steady states of deterministic dynamical systems and stochastic processes.[2–16] Here, we have a stochastic process in a steady state and the random variable counts the numbers of reactive events. The prediction of the fluctuation theorem is that the generating function (64) obeys the fundamental symmetry relation

$$Q(\lambda) = Q(A - \lambda) \tag{68}$$

where A is the chemomechanical affinity (41).[9] This symmetry relation can be verified in the case of the generating function (65) by noting that the chemomechanical affinity is given in terms of the transition rates by the relation[71]

$$\mathrm{e}^{A} = \frac{W_{+1}W_{+2}}{W_{-1}W_{-2}} \tag{69}$$

Similar considerations apply to the generating function of the substeps S_t performed by the motor during the time interval $[0, t]$:

$$\tilde{Q}(\xi) \equiv \lim_{t\to\infty} -\frac{1}{t}\ln\langle \mathrm{e}^{-\xi S_t}\rangle \tag{70}$$

Since the number of substeps is related to the number of reactive events by $S_t \simeq 2N_t$ over a long enough time interval, their respective generating functions are linked by $\tilde{Q}(\xi) = Q(2\xi)$ so that we also have the symmetry relation

$$\tilde{Q}(\xi) = \tilde{Q}\left(\frac{A}{2} - \xi\right) \tag{71}$$

as the consequence of the fluctuation theorem.[9]

It can be shown that the fluctuation theorem (71) can also be expressed as

$$\frac{P(S_t = +s)}{P(S_t = -s)} = \mathrm{e}^{As/2} \tag{72}$$

in terms of the probability $P(S_t = s)$ that the nanomotor rotates by $S_t = s$ substeps over a long enough time interval t.[9] This symmetry relation compares the probabilities of moving forward or backward. The ratio of the probabilities of opposite fluctuations is determined by the chemomechanical affinity (41). This latter vanishes at equilibrium in which case both probabilities are equal and the principle of detailed balance is satisfied. Out of equilibrium, the probability of moving in the direction of the affinity becomes larger than the probability of the opposite movement and a directionality emerges under the effect of the thermodynamic force. It is interesting to notice that the ratio behaves exponentially so that the probabilities of opposite movements may soon become extremely different as the system is driven out of equilibrium.

Equations (71) and (72) are equivalent expressions of the fluctuation theorem. Indeed, the average entering into the definition of the generating function (70) can be written as

$$\langle \mathrm{e}^{-\xi S_t}\rangle = \sum_{s=-\infty}^{+\infty} P(S_t = s)\,\mathrm{e}^{-\xi s} \tag{73}$$

Using Eq. (72) and performing the substitution $s \to -s$ into the sum, we find that

$$\sum_{s=-\infty}^{+\infty} P(S_t = s)\,\mathrm{e}^{-\xi s} = \sum_{s=-\infty}^{+\infty} P(S_t = s)\,\mathrm{e}^{-\left(\frac{A}{2}-\xi\right)s} \tag{74}$$

whereupon we get Eq. (71) in the long-time limit.[9]

The symmetry relation (72) can be verified by direct simulations of the discrete-state model (11)-(12) using the Gillespie algorithm.[74,75] Figure 10 depicts the probability distribution $P(S_t = s)$ that the F_1-ATPase nanomotor would rotate by a certain number $S_t = s$ of substeps over a time interval of 10 s for values of the external torque around the stalling torque (60) in a regime with a micromolar concentration of ATP and millimolar (or equivalent) concentrations of ADP and $\mathrm{P_i}$. For the given concentrations, the stalling torque (60) is equal to $\tau_{\mathrm{stall}} = -26.02$ pN nm. In Fig. 10, the external torque takes values below and above the stalling torque, in which cases the mean rotation rate is respectively negative and positive. We see that the dispersion around the mean value of the probability distribution is relatively important in this regime so that the probability of backward fluctuations remains substantial. We also observe the large difference in the probabilities of both states. At the stalling torque, the ratio of the probabilities (16)-(17) is equal to $P_1^{(\mathrm{st})}/P_2^{(\mathrm{st})} = 29.7$ so that the catalytic site is more often empty than occupied. This explains that the probability distribution takes alternating values over even and odd substeps, as seen in Fig. 10.

For both values of the external torque, the prediction of the fluctuation theorem (72) has been superimposed with crosses to the probability distribution $P(S_t = s)$, showing its equality with the reversed probability distribution multiplied by the exponential $P(S_t = -s)\,\mathrm{e}^{sA/2}$, here for time intervals t of the order of 10 s. This remarkable symmetry provides an understanding of the emergence of directionality in the rotation of the F_1 motor as the nonequilibrium

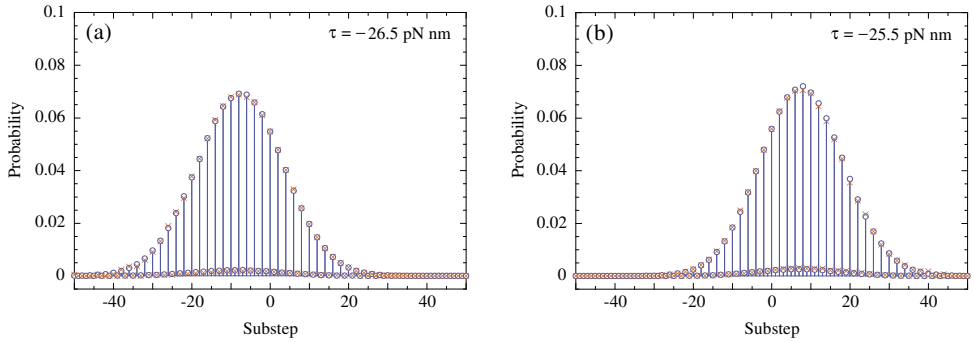

FIG. 10: Probability $P(S_t = s)$ (open circles) versus the number $S_t = s$ of substeps of rotation of the F_1 motor during the time interval $t = 10\,\mathrm{s}$ compared with the prediction $P(S_t = -s)\,e^{sA/2}$ (crosses) of the fluctuation theorem for $[\mathrm{ATP}] = 3 \times 10^{-6}\,\mathrm{M}$, $[\mathrm{ADP}][\mathrm{P_i}] = 10^{-6}\,\mathrm{M}^2$, and the torques: (a) $\tau = -26.5$ pN nm; (b) $\tau = -26.5$ pN nm. The diameter of the bead is $d = 2r = 80$ nm and the temperature of 23 degrees Celsius. For the given concentrations, the chemomechanical affinity (41) vanishes at the value $\tau_{\mathrm{stall}} = -26.02$ pN nm of the torque. The counting statistics is obtained by direct simulation with the Gillespie algorithm over 10^6 random trajectories of the discrete-state model (11)-(12).

constraints are switched on. The fluctuation theorem shows that the emergence of directionality out of the molecular fluctuations obeys a universal relation of thermodynamic origin and here associated with the tightness of the chemomechanical coupling in the F_1-ATPase motor.

Thanks to the control provided by the external torque, the chemomechanical affinity (41) can be tuned to small positive or negative values around the stalling torque in regimes where the backward fluctuations of the motor are abundant even over a relatively short time interval such as $t = 10$ s. In contrast, in the absence of an external torque, the backward fluctuations are rare at low values of the affinity for reasons similar to the ones discussed in Subsection IV B and very long time intervals of 10^4 s are required to obtain a significant statistics of backward fluctuations.[9] Therefore, the application of an external torque opens the possibility to test experimentally the steady-state fluctuation theorem in the reaction-limited regime of the F_1 motor. An appropriate experimental technique would be to induce the external torque on the γ-shaft by electrorotation,[30] which has the advantage of generating constant external torques. Until now, the experiment has been carried out in the absence of ADP and P_i, i.e., in a fully irreversible regime of infinite chemomechanical affinity $A = +\infty$ where the probability of opposite rotation vanishes, in consistency with the observations reported in Ref. 30. As predicted by the fluctuation theorem (72), the presence of ADP and P_i together with ATP is essential in order to observe both backward and forward rotations.

We notice that the fluctuation theorem (72) holds in the reaction-limited regime at low friction. In the opposite friction-limited regime, the power strokes are so damped by viscous friction that the reactive events no longer leave distinct jumps in the observed trajectories.[37] In this different regime, the rotation of the motor finds an effective description in terms of a simple Langevin process and another fluctuation theorem can be considered over the millisecond time scale of the mechanical fluctuations, as shown in Ref. 76.

The extension of the fluctuation theorem to regimes without tight coupling can also be carried out (cf. Ref. 13 and Appendix F).

V. CONCLUSIONS

In the present paper, we have studied the chemomechanical coupling and the efficiency of the F_1-ATPase nanomotor with an applied external torque from the viewpoint of stochastic thermodynamics. The chemomechanical coupling of motor proteins is determined by their 3D molecular architecture, which constrains the possible 4D space-time trajectories of the protein assembly. In this regard, the chemomechanical coupling is a property associated with the movements and kinetics of the motor protein in specific environments supplying chemical energy and dissipating mechanical work. Accordingly, motor proteins are open systems and their chemomechanical properties can be formulated thanks to nonequilibrium thermodynamics.

In this regard, a key feature is that two different rate processes are coupled together in the F_1-ATPase rotary motor: (1) the mechanical rotation of the γ-shaft in the barrel formed by the $(\alpha\beta)_3$ hexamer and (2) the chemical reaction of ATP hydrolysis or its reversal. Both processes are characterized by their rate, also called thermodynamic flux: (1) the rotation rate and (2) the reaction rate. At thermodynamic equilibrium, both rates vanish because of the principle of detailed balance. As a consequence, the functioning of the motor requires energy supply from the

thermodynamic forces in order to generate the fluxes. These so-called affinities[68–70] are respectively: (1) the external torque and (2) the chemical affinity or Gibbs free energy difference between reactants and products. As shown by Onsager,[67] interrelations between the fluxes and the forces can be established on the basis of microreversibility and the fundamental expression for the entropy production. Now, the chemomechanical coupling between both processes is the remarkable ability of the motor protein to generate the thermodynamic flux of one particular process thanks to the thermodynamic force of the other process. Therefore, nonequilibrium thermodynamics provides a fundamental framework to formulate the problem of chemomechanical coupling.

One of the main results of the paper is that, in the regime of tight coupling, the molecular motor is driven out of equilibrium by the unique chemomechanical affinity (41), which combines the external torque with the chemical potential difference of ATP hydrolysis. This is a direct consequence of the tight-coupling condition which implies the proportionality between both thermodynamic fluxes entering into the expression (38) for the entropy production, as we have demonstrated in Subsection II D and Appendix D. Therefore, thermodynamic considerations provide a clear criterion to define a tight chemomechanical coupling. A corollary of this result is that the chemical equilibrium can be displaced by the external torque applied to a motor functioning in a tight-coupling regime, as expressed in terms of the chemomechanical affinity (41).

However, motor proteins have nanometric sizes, which has important consequences. First, if the chemical potentials of the reactants and products can be supposed to be uniform in the large environment where the concentrations of ATP, ADP and P_i are kept constant, the difference of chemical potentials is localized inside the motor protein over a few nanometers or less, as it is the case in chemical reactions or electronic heterojunctions. This has for consequence that the fluxes have highly nonlinear dependences on the chemical affinity so that molecular motors are typically functioning away from Onsager's linear regime of nonequilibrium thermodynamics, a fact which is often overlooked in spite of its crucial importance. As shown in Subsection IV B and Fig. 5, the F_1 motor is extremely slow in the linear regime but instead reaches a useful rate in the nonlinear regime, which is more the feature of far-from-equilibrium systems than of close-to-equilibrium systems. This remarkable property allows the motor to rotate under physiological conditions at about 130 rev/s although it would be a million times slower if the motor was functioning in a linear regime. Accordingly, the recent results obtained for the nonlinear-response properties[77] are of great relevance to understand the function of nonequilibrium nanosystems such as molecular motors.

Another consequence of the nanometric size of motor proteins is that their movements are random at the molecular level and should be described in terms of stochastic processes. In the present paper, we have carried out a study of the F_1 motor by combining results from two levels of description. The finer description is provided by a continuous-angle stochastic model[37] which has previously been fitted to the experimental observations of Ref. 24. A coarser description is obtained in terms of discrete states corresponding to the steps and substeps observed in the rotary motion of the γ-shaft of F_1.[24] The discrete-state model is a Markovian jump process and its transition rates have been fitted by performing numerical simulations of the continuous-angle model using Gillespie algorithm.[74,75] An important aspect of our approach is that the discrete-state and continuous-angle models are linked together by coarse-graining the continuous space of the angle of the γ-shaft into the intervals corresponding to the observed substeps.[24] Since mechanical parameters such as the external torque and the friction coefficient are naturally introduced by the principles of Newtonian mechanics in the Fokker-Planck equations defining the continuous-angle model, an advantage of linking both levels of description is that we are able to determine the dependences of the discrete-state model on both the external torque and the friction coefficient.

In this way, we have shown that the transition rates are nearly independent of the friction coefficient in the reaction-limited regime at low friction and they decrease as the inverse of the friction coefficient at high friction. The analytical expression (51) has been obtained which takes these features into account in the crossover between the reaction-limited and friction-limited regimes. Moreover, a general dependence on the external torque has been considered in Eqs. (51)-(53), which guarantees the positivity of the transition rates. This form extends the simple exponential dependence which is often supposed but which is an approximation of the real dependence on the external torque or force. As seen in Table III, corrections to the exponential dependence turn out to be significant, especially, in the reaction-limited regime.

Thanks to the solvability of the two-state model, the stationary solutions of the master equation can be exactly deduced, allowing us to show analytically that the mean rotation rate obeys a Michaelis-Menten kinetics with respect to the ATP concentration in agreement with the experimental observations of Ref. 24 (see Fig. 4). Moreover, the analytical formula (22) is obtained for the rotation rate in the presence of both ATP and the products of ATP hydrolysis, i.e., ADP and P_i. The numerical simulations of the continuous-angle model are well described by Eq. (22) of the discrete-state model as seen in Fig. 6, which shows that the mean rotation rate decreases as the concentrations of ADP and P_i exceed a crossover value. The reason is that the release of the products of ATP hydrolysis in the motor is counteracted by the reverse reaction of the binding of products to the catalytic sites, which has the effect of slowing down the motor.

Furthermore, our combined study of both models allows us to identify the regime of tight chemomechanical coupling

in the F_1-ATPase nanomotor. Indeed, the discrete-state model presupposes that the mechanical motion and the chemical reaction powering the motor are tightly coupled, although the continuous-angle model does not. Accordingly, the comparison between both models clearly reveal the regime of tight coupling between mechanics and chemistry, as shown in Subsection IV A. The tight coupling manifests itself at moderate values of both the external torque and the chemical affinity, as observed in Fig. 2. This is probably due to the cylindrical architecture of the F_1 rotary motor and the ability of the γ-subunit to rotate inside the $(\alpha\beta)_3$ hexamer with neither too much freedom nor sticking and under the control of the chemical states of the catalytic sites in the β-subunit.

As the consequence of the tightness of the chemomechanical coupling, the mechanical efficiency can reach its optimal value, as shown in Subsection IV F and Fig. 9. Moreover, the chemical and mechanical efficiencies can culminate at their maximal unit value near the stalling torque. The coupling between mechanics and chemistry is so tight that the expected deviations between the stalling torque and the values of the torque where the efficiencies reach their maximum value turn out to be very small. The coincidence of these different values of the external torque is the consequence of the high degree of tight coupling achieved in the F_1 motor, but would not necessarily hold for a motor functioning in a loose-coupling regime.

Another of the main results of this paper is the demonstration carried out in Subsection IV G that the fluctuation theorem can be used to characterize the random rotations of the F_1 motor in the tight-coupling regime with an applied external torque. The fluctuation theorem allows us to establish a universal relation (72) between the probabilities of random movements in opposite directions and the chemomechanical affinity (41) of nonequilibrium thermodynamics. This remarkable symmetry relation is valid arbitrarily far from equilibrium and is a consequence of the microreversibility underlying the dynamics of the F_1 motor in its environment.[2–16] At equilibrium, the chemomechanical affinity vanishes and the principle of detailed balance is recovered. Out of equilibrium, the fluctuation theorem provides a thermodynamic explanation for the emergence of directionality from the fluctuations of the motor. The sign of the chemomechanical affinity together with the second law of thermodynamics and the chirality of the motor protein determines the mean forward direction of rotation. The nonequilibrium driving given by the chemomechanical affinity generates a bias among the fluctuations of the motor, the forward substeps becoming more probable than the backward ones, as strikingly described by the fluctuation theorem (72). Thanks to the external torque, the motor can be driven in regimes near the stalling torque where both forward and backward fluctuations are abundant if ATP together with the products of its hydrolysis, ADP and P_i, are supplied to the motor environment. This should create suitable conditions under which the experimental test of the steady-state fluctuation theorem could be feasible in the reaction-limited regime of the F_1 motor with the technique of electrorotation.[30] Thanks to the fluctuation theorem, fundamental thermodynamic properties of the F_1-ATPase motor such as the chemomechanical affinity should become accessible to experimental measurements.[63]

Acknowledgments

P. Gaspard wishes to acknowledge a discussion with K. Hayashi about the technique of electrorotation. E. Gerritsma is grateful to the "Fonds pour la Formation à la Recherche dans l'Industrie et l'Agriculture" (F. R. I. A. Belgium) for financial support. This research has also been supported by the Belgian Federal Government (IAP project "NOSY"), the "Communauté française de Belgique" (contract "Actions de Recherche Concertées" No. 04/09-312), and the F. R. S.-FNRS Belgium (contract F. R. F. C. No. 2.4577.04).

APPENDIX A: COARSE-GRAINING METHODS

Besides the direct numerical method of Subsection II C used in the present paper to fit the discrete-state model, there also exist analytical methods to reduce continuous-state processes defined by coupled Fokker-Planck equations such as Eqs. (43) to discrete-state processes ruled by the master equation (10). Here below, we first describe a method based on the separation of time scales between the short reactive jumps and the longer plateaus in the chemical states. The second method is using the projection-operator method of nonequilibrium statistical mechanics[73] and can be used to improve the first one.

1. Reduction to a jump process at low friction

In the reaction-limited regime at low friction ζ, the jump times are shorter than the dwell times in each potential well. In this case, the Fokker-Planck equations (43) can be written as

$$\partial_t\, p_\nu(\theta,t) + \frac{1}{\zeta}\,\partial_\theta\, K_\nu(\theta,t) = \sum_{\nu'} p_{\nu'}(\theta,t)\;\omega_{\nu'\nu}(\theta) \tag{A1}$$

where

$$K_\nu(\theta,t) = -k_{\rm B}T\;\partial_\theta\, p_\nu(\theta,t) - [\partial_\theta U_\nu(\theta) - \tau]\, p_\nu(\theta,t) \tag{A2}$$

The potentials are periodic $U_\nu(\theta) = U_\nu(\theta+2\pi)$, as well as the angle-dependent transition rates $\omega_{\nu'\nu}(\theta) = \omega_{\nu'\nu}(\theta+2\pi)$. The probability densities are expanded in powers of the friction coefficient ζ and, as a consequence, the rescaled current densities as well:

$$p_\nu \;=\; p_\nu^{(0)} + \zeta\, p_\nu^{(1)} + \zeta^2\, p_\nu^{(2)} + \cdots \tag{A3}$$

$$K_\nu \;=\; K_\nu^{(0)} + \zeta\, K_\nu^{(1)} + \zeta^2\, K_\nu^{(2)} + \cdots \tag{A4}$$

Substituting these expansions in the Fokker-Planck equations (A1), we obtain equations at successive perturbative orders:

$$O(\zeta^0) \qquad \partial_\theta\, K_\nu^{(0)} = 0 \tag{A5}$$

$$O(\zeta^1) \qquad \partial_t\, p_\nu^{(0)} + \partial_\theta\, K_\nu^{(1)} = \sum_{\nu'} p_{\nu'}^{(0)}\;\omega_{\nu'\nu} \tag{A6}$$

$$\vdots$$

At zeroth order, Eq. (A5) expresses the steadiness of the probability current densities on each potential surface in the limit without any reactive transition between them. Since Eq. (A5) is linear in the function $p_\nu^{(0)}(\theta) \propto \phi_\nu(\theta)$, its solution is the eigenfunction of the following differential equation:

$$\frac{d}{d\theta}\left[\frac{d\phi_\nu}{d\theta} + \frac{1}{k_{\rm B}T}\left(\frac{dU_\nu}{d\theta} - \tau\right)\phi_\nu\right] = \lambda\,\phi_\nu \tag{A7}$$

corresponding to a vanishing eigenvalue $\lambda = 0$. Because of its periodicity $\phi_\nu(\theta+2\pi) = \phi_\nu(\theta)$, the solution is given by

$$\phi_\nu(\theta) = C_\nu\,{\rm e}^{-\upsilon_\nu(\theta)}\left[1 + \left({\rm e}^{-\frac{2\pi\tau}{k_{\rm B}T}} - 1\right)\frac{\int_0^\theta {\rm e}^{\upsilon_\nu(\theta')}d\theta'}{\int_0^{2\pi} {\rm e}^{\upsilon_\nu(\theta')}d\theta'}\right] \tag{A8}$$

with some normalization constant C_ν and

$$\upsilon_\nu(\theta) \equiv \frac{1}{k_{\rm B}T}\,[U_\nu(\theta) - \tau\theta] = \upsilon_\nu(\theta+2\pi) + \frac{2\pi\tau}{k_{\rm B}T} \tag{A9}$$

If the external torque vanishes $\tau = 0$, the solution reduces to a Boltzmann equilibrium distribution in the free-energy potential $U_\nu(\theta)$.

We also consider the associated function $\psi_\nu(\theta)$ such that

$$\begin{aligned} 0 = \langle\psi_\nu|\partial_\theta K_\nu\rangle \;&=\; \int_0^{2\pi} \psi_\nu^*\,\partial_\theta\left[-k_{\rm B}T\;\partial_\theta\, f_\nu - (\partial_\theta U_\nu - \tau)\, f_\nu\right] d\theta \\ &=\; \left\{\int_0^{2\pi} f_\nu^*\left[-k_{\rm B}T\;\partial_\theta^2\,\psi_\nu + (\partial_\theta U_\nu - \tau)\,\partial_\theta\psi_\nu\right] d\theta\right\}^* \end{aligned} \tag{A10}$$

for arbitrary functions $f_\nu(\theta)$ and satisfying the normalization condition $\langle\psi_\nu|\phi_\nu\rangle = \int_0^{2\pi}\psi_\nu^*\phi_\nu d\theta = 1$. The associated function obeys the differential equation:

$$\frac{d^2\psi_\nu}{d\theta^2} - \frac{1}{k_{\rm B}T}\left(\frac{dU_\nu}{d\theta} - \tau\right)\frac{d\psi_\nu}{d\theta} = \lambda^*\,\psi_\nu \tag{A11}$$

with $\lambda = 0$. For periodic boundary conditions, the solution of this equation is just a constant which can be taken equal to unity, $\psi_\nu(\theta) = 1$.

The discrete-state probabilities are introduced as the proportionality constants at given time t between the zeroth-order probability densities and the eigensolutions (A8):

$$p_\nu^{(0)}(\theta,t) = P_\nu(t)\,\phi_\nu(\theta) \tag{A12}$$

so that

$$P_\nu(t) = \langle\psi_\nu|p_\nu^{(0)}\rangle = \int_0^{2\pi} p_\nu^{(0)}(\theta,t)\,d\theta \tag{A13}$$

Now, Eq. (A6) at first order can be multiplied by $\psi_\nu^* = 1$ and integrated over $\theta \in [0, 2\pi[$ to get

$$\underbrace{\langle\psi_\nu|\partial_t\, p_\nu^{(0)}\rangle}_{=dP_\nu/dt} + \underbrace{\langle\psi_\nu|\partial_\theta\, K_\nu^{(1)}\rangle}_{=0} = \sum_{\nu'}\langle\psi_\nu|p_{\nu'}^{(0)}\;\omega_{\nu'\nu}\rangle \tag{A14}$$

In the left-hand side, the first term is the time derivative of the discrete-state probability (A13) and the second term vanishes because the function ψ_ν satisfies Eq. (A10) for $f_\nu = p_\nu^{(1)}$. We thus find the master equation

$$\frac{dP_\nu(t)}{dt} = \sum_{\nu'} P_{\nu'}(t)\,\Omega_{\nu'\nu} \tag{A15}$$

with the transition rates

$$\Omega_{\nu'\nu} = \langle\psi_\nu|\phi_{\nu'}\,\omega_{\nu'\nu}\rangle = \int_0^{2\pi} \phi_{\nu'}(\theta)\,\omega_{\nu'\nu}(\theta)\,d\theta \tag{A16}$$

which are given by integrating the angle-dependent transition rates of the continuous process with the solutions (A8). The master equation (A15) can be further reduced by using the three-fold symmetry of the F_1 motor to finally obtain Eq. (10) ruling the time evolution of the discrete-state probabilities (50). Higher-order corrections can be analyzed similarly.

2. Projection-operator method

The projection-operator method[73] allows us to go beyond the leading-order master equation (A15). The probability densities are decomposed as

$$p_\nu(\theta,t) = P_\nu(t)\,\phi_\nu(\theta) + \chi_\nu(\theta,t) \tag{A17}$$

where the functions $\phi_\nu(\theta)$ are given by Eq. (A8) and the functions $\chi_\nu(\theta,t)$ are corrections such that $\int_0^{2\pi}\chi_\nu(\theta,t)\,d\theta = 0$ in order to get $P_\nu(t) = \int_0^{2\pi} p_\nu(\theta,t)\,d\theta$. This decomposition is carried out by projecting the probability densities onto the subspace of functions which are multiples of the solutions (A8):

$$\mathbf{p} = \{p_\nu(\theta,t)\} \longrightarrow \mathsf{P}\mathbf{p} = \left\{\phi_\nu(\theta)\int_0^{2\pi} p_\nu(\theta',t)\,d\theta'\right\} \tag{A18}$$

which defines the projection operator P. The complementary projector $\mathsf{Q} = \mathsf{1} - \mathsf{P}$ maps the probability densities onto the corrections $\{\chi_\nu(\theta,t)\}$. These projection operators satisfy

$$\mathsf{P}^2 = \mathsf{P} \qquad \mathsf{Q}^2 = \mathsf{Q} \qquad \mathsf{PQ} = \mathsf{QP} = 0 \tag{A19}$$

Using these properties, the linear system of the coupled Fokker-Planck equations (A1)

$$\partial_t\mathbf{p} = \mathsf{L}\mathbf{p} \tag{A20}$$

can be decomposed as[73]

$$\partial_t\begin{pmatrix}\mathsf{Pp}\\ \mathsf{Qp}\end{pmatrix} = \begin{pmatrix}\mathsf{PLP} & \mathsf{PLQ}\\ \mathsf{QLP} & \mathsf{QLQ}\end{pmatrix}\begin{pmatrix}\mathsf{Pp}\\ \mathsf{Qp}\end{pmatrix} \tag{A21}$$

The equation on the second line for the component $\mathbf{Qp}$ is solved to get

$$\mathbf{Qp}_t = \mathrm{e}^{\mathbf{QLQ}t}\,\mathbf{Qp}_0 + \int_0^t d\tau\,\mathrm{e}^{\mathbf{QLQ}\tau}\mathbf{QLP}\,\mathbf{Pp}_{t-\tau} \tag{A22}$$

Supposing that the initial conditions are such that $\mathbf{Qp}_0 = 0$ and substituting Eq. (A22) into the first line of Eq. (A21), we obtain

$$\partial_t \mathbf{Pp}_t = \mathbf{PLP}\,\mathbf{Pp}_t + \int_0^t d\tau\,\mathbf{PLQ}\,\mathrm{e}^{\mathbf{QLQ}\tau}\mathbf{QLP}\,\mathbf{Pp}_{t-\tau} \tag{A23}$$

Since the discrete-state probabilities are given by $P_\nu(t) = \langle\psi_\nu|\mathbf{Pp}_t\rangle$, we find the master equation

$$\frac{dP_\nu(t)}{dt} = \sum_{\nu'}\langle\psi_\nu|\mathbf{PLP}|\phi_{\nu'}\rangle P_{\nu'}(t) + \sum_{\nu'}\int_0^t d\tau\langle\psi_\nu|\mathbf{PLQ}\,\mathrm{e}^{\mathbf{QLQ}\tau}\mathbf{QLP}|\phi_{\nu'}\rangle P_{\nu'}(t-\tau) \tag{A24}$$

which is non-Markovian because of the memory term. This non-Markovian master equation is exact and forms a closed equation for the time evolution of the discrete-state probabilities $\{P_\nu(t)\}$. If the memory term is negligible, we recover Eq. (A15) with the transition rates (A16) since $\Omega_{\nu'\nu} = \langle\psi_\nu|\mathbf{PLP}|\phi_{\nu'}\rangle$. If the corrections are perturbative and their relaxation time is short enough, the memory of the past extends over a short time interval and the Markovian property is restored over long time scales. In this regard, the separation of time scales justifies the coarse graining of the continuous-variable stochastic process into a discrete-state one.

APPENDIX B: THERMODYNAMIC ENTROPY PRODUCTION

The laws of thermodynamics allow us to obtain the balance equations for the energy and entropy of the motor. In open systems such as molecular motors, energy and entropy vary because of exchanges with the surrounding medium and possible internal variations:

$$dE = d_{\mathrm{e}}E + d_{\mathrm{i}}E \tag{B1}$$

$$dS = d_{\mathrm{e}}S + d_{\mathrm{i}}S \tag{B2}$$

The laws of thermodynamics only rule the internal variations:

$$\text{first law:} \qquad d_{\mathrm{i}}E = 0 \tag{B3}$$

$$\text{second law:} \qquad d_{\mathrm{i}}S \geq 0 \tag{B4}$$

Since the motor exchanges heat and molecules with its environment and may be subjected to an external torque τ, its energy varies according to the balance equation:

$$dE = dQ + \tau\,d\theta + \sum_{\mathrm{X}}\mu_{\mathrm{X}}\,dN_{\mathrm{X}} \tag{B5}$$

where dQ is the heat exchanged with the environment, $d\theta$ the rotation angle, dN_{X} the number of molecules of species X entering the motor, and μ_{X} the corresponding chemical potential (3) with X = ATP, ADP, or $\mathrm{P_i}$. The changes in molecular numbers due to the overall reaction (1) satisfy

$$dN_{\mathrm{ATP}} = -dN_{\mathrm{ADP}} = -dN_{\mathrm{P_i}} \tag{B6}$$

so that the balance equation (B5) can be expressed as

$$dE = dQ + \tau\,d\theta + \Delta\mu\,dN_{\mathrm{ATP}} \tag{B7}$$

in terms of the chemical potential difference (2) of the overall reaction. Moreover, the heat exchanged with the environment is related to the exchange of entropy by $dQ = Td_{\mathrm{e}}S$. Since energy and entropy are state variables, they recover their starting value after the motor has completed a cyclic path, whereupon their integration over a cycle vanishes, $\oint dE = 0$ and $\oint dS = 0$. For the isothermal process of a nanomotor functioning in the heat bath formed by the surrounding medium, the entropy irreversibly produced over a cycle of the motor is thus given by

$$\oint d_{\mathrm{i}}S = -\oint d_{\mathrm{e}}S = \frac{1}{T}\oint(\tau\,d\theta + \Delta\mu\,dN_{\mathrm{ATP}}) \geq 0 \tag{B8}$$

which is obtained by using Eqs. (B2), (B4), and (B7) for the cyclic path.

Averaging over many cycles in a stationary regime, the formula (38) is deduced for the thermodynamic entropy production in terms of the rotation and reaction rates, Eqs. (18) and (19).

APPENDIX C: AFFINITIES AND CURRENTS

The molecular motor can be driven out of equilibrium by the two independent affinities which are the mechanical and the chemical affinities, respectively proportional to the torque τ and the chemical potential difference $\Delta\mu$. These affinities and the corresponding fluxes or currents can be defined as

$$A_{\rm m} \equiv \frac{2\pi}{3}\frac{\tau}{k_{\rm B}T} \quad \longleftrightarrow \quad J_{\rm m} \equiv 3V \tag{C1}$$

$$A_{\rm c} \equiv \frac{\Delta\mu}{k_{\rm B}T} \quad \longleftrightarrow \quad J_{\rm c} \equiv R \tag{C2}$$

in which case the thermodynamic entropy production (38) takes the following form:

$$\frac{1}{k_{\rm B}}\frac{d_{\rm i}S}{dt} = A_{\rm m}J_{\rm m} + A_{\rm c}J_{\rm c} \geq 0 \tag{C3}$$

In general, the currents are nonlinear functions of the affinities

$$J_{\rm m} = J_{\rm m}(A_{\rm m}, A_{\rm c}) \tag{C4}$$

$$J_{\rm c} = J_{\rm c}(A_{\rm m}, A_{\rm c}) \tag{C5}$$

which vanish at the thermodynamic equilibrium where the affinities vanish, $A_{\rm m} = A_{\rm c} = 0$.[67–71] Close to equilibrium, the currents can be expanded in powers of the affinities, which defines the linear-response coefficients L_{ij} as

$$J_{\rm m} = L_{11}A_{\rm m} + L_{12}A_{\rm c} + O(2) \tag{C6}$$

$$J_{\rm c} = L_{21}A_{\rm m} + L_{22}A_{\rm c} + O(2) \tag{C7}$$

The microreversibility implies the Onsager reciprocity relation[67]

$$L_{12} = L_{21} \tag{C8}$$

and the non-negativity of the entropy production (C3) the inequality

$$L_{11}L_{22} \geq L_{12}^2 \qquad \text{with} \quad L_{11}, L_{22} \geq 0 \tag{C9}$$

The coupling between mechanics and chemistry is here possible because the motor is attached to a solid support and keeps a fixed orientation. Consequently, chemistry becomes vectorial as it is the case for mechanics. There is thus no contradiction with the Curie symmetry principle according to which scalar and vectorial processes cannot be coupled together.[68,69] In isotropic media such as liquids, chemistry is scalar and cannot be coupled to mechanics which is vectorial. This coupling becomes possible if the medium is anisotropic as in liquid crystals or in proteins attached to the surface of a solid.

In the plane of the affinities $(A_{\rm m}, A_{\rm c})$, the curve where the velocity vanishes behaves around the origin as

$$J_{\rm m} = 3V = 0: \qquad A_{\rm c} = -\frac{L_{11}}{L_{12}}A_{\rm m} + O(A_{\rm m}^2) \tag{C10}$$

while the curve where the ATP consumption rate vanishes is given by

$$J_{\rm c} = R = 0: \qquad A_{\rm c} = -\frac{L_{21}}{L_{22}}A_{\rm m} + O(A_{\rm m}^2) \tag{C11}$$

Near the origin, the curve (C10) has a more negative slope than the curve (C11) as the consequence of the inequality (C9) resulting from the second law of thermodynamics.[33]

APPENDIX D: THERMODYNAMIC IMPLICATIONS OF TIGHT COUPLING

In the case of tight coupling between the mechanics and the chemistry of the molecular motor, the two curves (C10) and (C11) have the same slope around the thermodynamic equilibrium point. Indeed, the tight-coupling condition (39) reads

$$J_{\rm m} = J_{\rm c} \equiv J \tag{D1}$$

so that the entropy production becomes

$$\frac{1}{k_{\rm B}}\frac{d_{\rm i}S}{dt} = AJ \geq 0 \tag{D2}$$

with the chemomechanical affinity (41), which here reads

$$A \equiv A_{\rm m} + A_{\rm c} \tag{D3}$$

Therefore, the mechanical and chemical affinities are no longer independent in the tight-coupling regime where the chemomechanical affinity (D3) becomes the unique nonequilibrium driving force. Accordingly, the unique current (D1) is a function of this unique affinity:

$$J = J(A) = LA + O(A^2) \tag{D4}$$

and all the linear-response coefficients become related to each other by

$$L \equiv L_{11} = L_{12} = L_{21} = L_{22} \tag{D5}$$

In this case, the inequality (C9) reaches the equality:

$$L_{11}L_{22} = L_{12}^2 \tag{D6}$$

which is also characteristic of tight coupling.

APPENDIX E: THE EFFICIENCIES IN THE LINEAR REGIME

The chemical and mechanical efficiencies (61)-(62) can be expressed as follows in terms of the affinities and the currents:

$$\eta_{\rm c} = -\frac{A_{\rm c}J_{\rm c}}{A_{\rm m}J_{\rm m}} = \frac{1}{\eta_{\rm m}} \tag{E1}$$

In the regime of linear response where the currents are the linear functions (C6)-(C7) of the affinities, the efficiencies can be written in the form

$$\eta_{\rm c} = -\frac{1-\varepsilon}{\alpha}\,\frac{\alpha+1}{\alpha+1-\varepsilon} = \frac{1}{\eta_{\rm m}} \tag{E2}$$

in terms of the coefficient

$$\alpha \equiv \frac{L_{12}}{L_{22}}\frac{A_{\rm m}}{A_{\rm c}} \tag{E3}$$

and the constant

$$\varepsilon \equiv 1 - \frac{L_{12}^2}{L_{11}L_{22}} \tag{E4}$$

such that $0 \leq \varepsilon \leq 1$ by the inequality (C9). Equations (E2) and (E3) show that the efficiencies only depend on the ratio of the affinities.[33] In their respective domains of variation, the chemical and mechanical efficiencies can reach the maximum value

$$0 \leq \eta_{\rm max} \equiv \frac{1-\sqrt{\varepsilon}}{1+\sqrt{\varepsilon}} \leq 1 \tag{E5}$$

This happens along different curves in the plane $(A_{\rm m}, A_{\rm c})$ of the affinities with respect to the curves where the rotation and ATP consumption rates vanish since[33]

$$\eta_{\rm m} = \eta_{\rm max} \quad \text{if} \quad \alpha = -1 + \sqrt{\varepsilon} \tag{E6}$$

$$J_{\rm m} = 3V = 0 \quad \text{if} \quad \alpha = -1 + \varepsilon \tag{E7}$$

$$J_{\rm c} = R = 0 \quad \text{if} \quad \alpha = -1 \tag{E8}$$

$$\eta_{\rm c} = \eta_{\rm max} \quad \text{if} \quad \alpha = -1 - \sqrt{\varepsilon} \tag{E9}$$

In the tight-coupling limit, the coefficient (E4) vanishes because of Eq. (D6), $\varepsilon = 0$, so that the chemical and mechanical efficiencies take the value

$$\eta_{\rm c} = \frac{1}{\eta_{\rm m}} = -\frac{1}{\alpha} = -\frac{A_{\rm c}}{A_{\rm m}} \tag{E10}$$

according to Eqs. (D5) and (E2). In this case, the four conditions (E6)-(E9) coincide in $\alpha = -1$ where the chemical and mechanical efficiencies reach their maximal value which is equal to unity, $\eta_{\max} = 1$. Therefore, tight coupling favors the optimization of the efficiencies.

APPENDIX F: THE FLUCTUATION THEOREM

The fluxes or currents defined by Eqs. (C1) and (C2) are the statistical averages of fluctuating fluxes $j_{\rm m}(t)$ and $j_{\rm c}(t)$. Their integral over the time interval $[0,t]$ are related by Eqs. (18) and (19) to the angle $\theta(t)$ of rotation and the number $N_{\rm ATP}(t)$ of ATP molecules which have entered the catalytic sites during the time interval $[0,t]$ according to:

$$G_{\rm m}(t) \equiv \int_0^t j_{\rm m}(t')\,dt' = \frac{3}{2\pi}\,\theta(t) \tag{F1}$$

$$G_{\rm c}(t) \equiv \int_0^t j_{\rm c}(t')\,dt' = N_{\rm ATP}(t) \tag{F2}$$

The bivariate generating function of the counting statistics of these fluctuating quantities is defined by

$$\mathcal{Q}(\lambda_{\rm m},\lambda_{\rm c}) \equiv \lim_{t\to\infty} -\frac{1}{t}\ln\langle {\rm e}^{-\lambda_{\rm m}G_{\rm m}(t)-\lambda_{\rm c}G_{\rm c}(t)}\rangle = \lim_{t\to\infty} -\frac{1}{t}\ln\langle {\rm e}^{-\lambda_{\rm m}\frac{3}{2\pi}\theta(t)-\lambda_{\rm c}N_{\rm ATP}(t)}\rangle \tag{F3}$$

where $\lambda_{\rm m}$ and $\lambda_{\rm c}$ are parameters for expanding the generating function into cumulants.[10] Under general conditions, the fluctuation theorem for the currents[10] establishes the bivariate symmetry relation

$$\mathcal{Q}(\lambda_{\rm m},\lambda_{\rm c}) = \mathcal{Q}(A_{\rm m}-\lambda_{\rm m},A_{\rm c}-\lambda_{\rm c}) \tag{F4}$$

in terms of the mechanical and chemical affinities given by Eqs. (C1) and (C2).

Now, the tight-coupling condition states that the mechanical movements are directly controlled by the chemical reactions so that

$$G_{\rm m}(t) = G_{\rm c}(t) \tag{F5}$$

This tight chemomechanical coupling implies that the bivariate generating function becomes a function of the sole parameter

$$\lambda \equiv \lambda_{\rm m} + \lambda_{\rm c} \tag{F6}$$

because

$$\mathcal{Q}(\lambda_{\rm m},\lambda_{\rm c}) = \lim_{t\to\infty} -\frac{1}{t}\ln\langle {\rm e}^{-(\lambda_{\rm m}+\lambda_{\rm c})G_{\rm c}(t)}\rangle = Q(\lambda_{\rm m}+\lambda_{\rm c}) = Q(\lambda) \tag{F7}$$

and we recover the generating function defined by Eq. (64). Consequently, under the tight-coupling condition, the bivariate symmetry relation (F4) reduces to the simple symmetry relation (68) in terms of the unique chemomechanical affinity (D3).

The general bivariate symmetry relation (F4) is equivalent to the property

$$\frac{\mathcal{P}(G_{\rm m},G_{\rm c})}{\mathcal{P}(-G_{\rm m},-G_{\rm c})} = {\rm e}^{A_{\rm m}G_{\rm m}+A_{\rm c}G_{\rm c}} \tag{F8}$$

holding for the probability $\mathcal{P}(G_{\rm m},G_{\rm c})$ that the fluctuating quantities (F1) and (F2) take given values over a long enough time interval. Under the tight-coupling condition that the fluctuating quantities are linked to each other by $G_{\rm m} = G_{\rm c} \equiv G$, the bivariate fluctuation theorem (F8) reduces to the symmetry relation

$$\frac{P(G)}{P(-G)} = {\rm e}^{AG} \tag{F9}$$

in terms of the probability $P(G) \equiv \mathcal{P}(G_{\rm m} = G, G_{\rm c} = G)$ and the chemomechanical affinity (D3). The symmetry relations (F9) or (72) in terms of a single fluctuating variable are thus characteristic of the regime of tight coupling. In the regime of loose coupling, only the bivariate symmetry relation (F8) holds, which provides a possible test of the tightness of the chemomechanical coupling.

We notice that these results have consequences on the nonlinear-response properties studied in Ref. 77. Since the fluctuation theorem is valid arbitrarily far from equilibrium, the present results extend the considerations based on Eqs. (C6) and (C7), which were restricted to the regime of linear response close to equilibrium.

[1] C. Y. Mou, J.-L. Luo, and G. Nicolis, J. Chem. Phys. **84**, 7011 (1986).
[2] D. J. Evans, E. G. D. Cohen, and G. P. Morriss, Phys. Rev. Lett. **71**, 2401 (1993).
[3] G. Gallavotti and E. G. D. Cohen, Phys. Rev. Lett. **74**, 2694 (1995).
[4] G. E. Crooks, Phys. Rev. E **60**, 2721 (1999).
[5] J. L. Lebowitz and H. Spohn, J. Stat. Phys. **95**, 333 (1999).
[6] P. Gaspard, J. Chem. Phys. **120**, 8898 (2004).
[7] U. Seifert, Europhys. Lett. **70**, 36 (2005).
[8] U. Seifert, Phys. Rev. Lett. **95**, 040602 (2005).
[9] D. Andrieux and P. Gaspard, Phys. Rev. E **74**, 011906 (2006).
[10] D. Andrieux and P. Gaspard, J. Stat. Phys. **127**, 107 (2007).
[11] A. W. C. Lau, D. Lacoste, and K. Mallick, Phys. Rev. Lett. **99**, 158102 (2007).
[12] D. Lacoste, A. W. C. Lau, and K. Mallick, Phys. Rev. E **78**, 011915 (2008).
[13] D. Lacoste and K. Mallick, Phys. Rev. E **80**, 021923 (2009).
[14] C. Jarzynski, Eur. Phys. J. B **64**, 331 (2008).
[15] U. Seifert, Eur. Phys. J. B **64**, 423 (2008).
[16] M. Esposito, U. Harbola, and S. Mukamel, Rev. Mod. Phys. **81**, 1665 (2009).
[17] T. L. Hill, *Free Energy Transduction and Biochemical Cycle Kinetics* (Dover, New York, 2005).
[18] J. P. Abrahams, A. G. W. Leslie, R. Lutter, and J. E. Walker, Nature **370**, 621 (1994).
[19] R. I. Menz, J. E. Walker, and A. G. W. Leslie, Cell **106**, 331 (2001).
[20] B. Alberts, D. Bray, A. Johnson, J. Lewis, M. Raff, K. Roberts, and P. Walter, *Essential Cell Biology* (Garland Publishing, New York, 1998).
[21] C. von Ballmoos, G. M. Cook, and P. Dimroth, Annu. Rev. Biophys. **37**, 43 (2008).
[22] W. Junge, H. Sielaff, and S. Engelbrecht, Nature **459**, 364 (2009).
[23] H. Noji, R. Yasuda, M. Yoshida, and K. Kinosita Jr., Nature **386**, 299 (1997).
[24] R. Yasuda, H. Noji, M. Yoshida, K. Kinosita Jr., and H. Itoh, Nature **410**, 898 (2001).
[25] K. Kinosita Jr., K. Adachi, and H. Itoh, Annu. Rev. Biophys. Biomol. Struct. **33**, 245 (2004).
[26] K. Adachi, K. Oiwa, T. Nishizaka, S. Furuike, H. Noji, H. Itoh, M. Yoshida, and K. Kinosita Jr., Cell **130**, 309 (2007).
[27] K. Shimabukuro, R. Yasuda, E. Muneyuki, K. Y. Hara, K. Kinosita Jr., and M. Yoshida, Proc. Natl. Acad. Sci. U. S. A. **100**, 14731 (2003).
[28] H. Itoh, A. Takahashi, K. Adachi, H. Noji, R. Yasuda, M. Yoshida, and K. Kinosita Jr., Nature **427**, 465 (2004).
[29] Y. Rondelez, G. Tresset, T. Nakashima, Y. Kato-Yamada, H. Fujita, S. Takeuchi, and H. Noji, Nature **433**, 773 (2005).
[30] T. Watanabe-Nakayama, S. Toyabe, S. Kudo, S. Sugiyama, M. Yoshida, and E. Muneyuki, Biochem. Biophys. Research Commun. **366**, 951 (2008).
[31] A. B. Kolomeisky and M. E. Fisher, Annu. Rev. Phys. Chem. **58**, 675 (2007).
[32] R. D. Astumian and M. Bier, Phys. Rev. Lett. **72**, 1766 (1994).
[33] F. Jülicher, A. Ajdari, and J. Prost, Rev. Mod. Phys. **69**, 1269 (1997).
[34] H. Wang and G. Oster, Nature **396**, 279 (1998).
[35] H. Qian, J. Math. Chem. **27**, 219 (2000).
[36] M. S. Liu, B. D. Todd, and R. J. Sadus, J. Chem. Phys. **118**, 9890 (2003).
[37] P. Gaspard and E. Gerritsma, J. Theor. Biol. **247**, 672 (2007).
[38] L. Xu, Biochim. Biophys. Acta Bioenergetics **1777**, 1422 (2008).
[39] P. Xie, Biochim. Biophys. Acta Bioenergetics **1787**, 955 (2009).
[40] D. Keller and C. Bustamante, Biophys. J. **78**, 541 (2000).
[41] R. Lipowsky, Phys. Rev. Lett. **85**, 4401 (2000).
[42] R. Lipowsky and N. Jaster, J. Stat. Phys. **110**, 1141 (2003).
[43] H. Wang, C. Peskin, and T. Elston, J. Theor. Biol. **221**, 491 (2003).
[44] J. Xing, H. Wang, and G. Oster, Biophys. J. **89**, 1551 (2005).
[45] G. Lattanzi and A. Maritan, Phys. Rev. E **64**, 061905 (2001).
[46] G. Lattanzi and A. Maritan, J. Chem. Phys. **117**, 10339 (2002).
[47] C. Maes and M. H. van Wieren, J. Stat. Phys. **112**, 329 (2003).
[48] S. Liepelt and R. Lipowsky, Phys. Rev. Lett. **98**, 258102 (2007).
[49] S. Liepelt and R. Lipowsky, Europhys. Lett. **77**, 50002 (2007).

[50] R. Lipowsky and S. Liepelt, J. Stat. Phys. **130**, 39 (2008); *Erratum*, J. Stat. Phys. **135**, 777 (2009).
[51] A. Garai, D. Chowdhury, and M. D. Betterton, Phys. Rev. E **77**, 061910 (2008).
[52] G. Nicolis and I. Prigogine, *Self-Organization in Nonequilibrium Systems* (Wiley, New York, 1977).
[53] C. W. Gardiner, *Handbook of Stochastic Methods for Physics, Chemistry and the Natural Sciences*, 3rd edition (Springer, Berlin, 2004).
[54] G. Lattanzi and A. Maritan, Phys. Rev. Lett. **86**, 1134 (2001).
[55] M. E. Fisher and A. B. Kolomeisky, Proc. Natl. Acad. Sci. USA **96**, 6597 (1999).
[56] M. E. Fisher and A. B. Kolomeisky, Proc. Natl. Acad. Sci. USA **98**, 7748 (2001).
[57] T. Schmiedl and U. Seifert, Europhys. Lett. **83**, 30005 (2008).
[58] Y. Zhang, Physica A **388**, 3465 (2009).
[59] Y. C. Kim and M. E. Fisher, J. Phys.: Condens. Matter **17**, S3821 (2005).
[60] M. E. Fisher and Y. C. Kim, Proc. Natl. Acad. Sci. USA **102**, 16209 (2005).
[61] A. Valleriani, S. Liepelt and R. Lipowsky, Europhys. Lett. **82**, 28011 (2008).
[62] F. Oosawa and S. Hayashi, Adv. Biophys. **22**, 151 (1986).
[63] C. J. Bustamante, in: A. H. Zewail, Editor, *Physical Biology: From Atoms to Medicine* (Imperial College Press, London, 2008) pp. 115-135.
[64] N. Sakaki, R. Shimo-Kon, K. Adachi, H. Itoh, S. Furuike, E. Muneyuki, M. Yoshida, and K. Kinosita Jr., Biophys. J. **88**, 2047 (2005).
[65] P. Gaspard, Physica A **369**, 201 (2006).
[66] H. R. Horton, L. A. Moran, K. G. Scrimgeour, M. D. Perry, and J. D. Rawn, *Principles of Biochemistry*, 4th edition (Prentice Hall - Pearson Education, Upper Saddle River NJ, 2005).
[67] L. Onsager, Phys. Rev. **37**, 405 (1931).
[68] I. Prigogine, *Introduction to Thermodynamics of Irreversible Processes* (Wiley, New York, 1967).
[69] D. Kondepudi and I. Prigogine, *Modern Thermodynamics: From Heat Engines to Dissipative Structures* (Wiley, Chichester, 1998).
[70] H. B. Callen, *Thermodynamics and an Introduction to Thermostatistics*, 2nd edition (Wiley, New York, 1985).
[71] J. Schnakenberg, Rev. Mod. Phys. **48**, 571 (1976).
[72] A. J. Hunt, F. Gittes, and J. Howard, Biophys. J. **67**, 766 (1994).
[73] R. Zwanzig, *Nonequilibrium Statistical Mechanics* (Oxford University Press, 2001).
[74] D. T. Gillespie, J. Comput. Phys. **22**, 403 (1976).
[75] D. T. Gillespie, J. Phys. Chem. **81**, 2340 (1977).
[76] K. Hayashi, H. Ueno, R. Iino, and H. Noji, Phys. Rev. Lett. **104**, 218103 (2010).
[77] D. Andrieux and P. Gaspard, J. Stat. Mech. P02006 (2007).